MANAGEMENT OF LIGHT FOR PHOTOVOLTAIC APPLICATIONS

A THESIS SUBMITTED IN PARTIAL FULFILLEMENT OF

THE REQUIREMENTS FOR THE DEGREE OF

MASTER OF SCIENCE

by

Perrakis Giorgos

UNIVERSITY OF CRETE

DEPARTMENT OF MATERIALS SCIENCE AND TECHNOLOGY

April 2016

Supervisors:

Prof. Maria Kafesaki

Thesis committee:

Prof. Dimitris Papazoglou

Prof. Stelios Tzortzakis

Abstract

Due to the limitation and the rising cost of the fossil fuel supplies as well as the advances in nanotechnology, solar cells continue to be a hot topic nowadays. There is though a need for the solar cells to become thinner so as to reduce the cost and to minimize the charge carrier (electrons-holes) recombination before collection.

However, one of the largest drawbacks of thin film solar cells is the very small interaction time of the incoming wave with the absorbing layer, resulting to small absorption, and thus small current generated by the cells and small cell efficiency. One way to face this problem is to exploit the possibilities offered by the field of plasmonics, i.e. involvement of surface plasmon polariton (SPPs) structures in the solar cells. SPPs, both propagating and localized, are associated with high local fields and strong scattering, and have been shown unique in guiding and confining light at the nanoscale, being thus promising for enhancing the absorption inside thin film solar cells.

In this work we study numerically the possibilities and potential of plasmonic nanostructures embedded in silicon thin film solar cells to increase the absorption properties of the solar cells, and thus the solar cell efficiency. More specifically three approaches for enhancing absorption are examined. In the first approach, we examine the Localized Surface Plasmon Resonances (LSPRs) supported by metallic nanoparticles of different shapes and sizes and in different positions in the cells. In the second, we examine the Surface Plasmon Polaritons (SPPs) excited in the silicon-back-reflector interface when the interface is periodically nanostructured. In the third approach, metallic and/or dielectric nanoparticles are placed on top of the solar cell and their potential to minimize the solar cell back reflection (enhancing thus the absorption) is examined.

As the above study showed, all the above approaches can constitute promising paths to increase the thin film solar cell efficiency.

Table of Contents

Acknowledgements

I would like to express my very great appreciation to Prof. Maria Kafesaki, Dr. George Kenanakis, Prof. Eleftherios Economou and Prof. Costas Soukoulis for their patience, support and the answers to my endless questions. Without their guidance the completion of this master's thesis would be impossible.

I would also like to thank all the members of the Photonic- Phononic- and Metamaterials (PPM) group. Their help, and support was invaluable.

Moreover, I would like to thank Prof. Stelios Tzortzakis and Prof. Dimitris Papazoglou for their presence in my thesis' committee.

Finally, I would like to thank the Foundation for Research and Technology - Hellas (FO.R.T.H.) for the financial support throughout my studies.

1 Introduction

1.1 Theory of solar cells

Sun is an important source of renewable energy in the form of radiant light and heat, therefore many technologies, like solar water heating and solar cells, take advantage of this phenomena to transform this energy to water heating or even electricity.

The study of solar cells specifically begun in the 19th century when it was observed that the presence of sunlight is capable of generating usable electrical energy[1]. Alexandre Edmond Becquerel in 1839 first observes this photovoltaic effect. According to this effect, some materials (semiconductors) absorb photons of light according to their bandgap and "release" electrons. These free electrons are captured, and an electric current results that can be used as electricity. B. Weston in 1888 proposed an apparatus which transforms radiant energy derived from the sun into electrical energy, or through electrical energy into mechanical energy; meantime, Wilhelm Hallwachs in 1904 makes a semiconductor-junction solar cell.

Nowadays, solar cells continue to be a hot topic because of the limitation and the rising cost of the fossil fuels supplies, in addition to the related environmental problems. Since we need to fulfill our energy needs using cost-effective and clean technologies, we need to enhance the absorption of solar cells, avoiding electricity loss, and reducing cost; improving this way the existing photovoltaic technologies.

In Fig. 1.1 we see how a solar cell operates. When two doped semiconductors, a p-type and an n-type (with free moving holes and electrons respectively) are brought in contact with each other, an electric field is formed. The electric field formed at equilibrium results from the barrier (opposite static charges left behind due to ionization of the atoms along the junction, by the tendency of the free electrons of the n-side to fill the free holes at the p-side) made at the pn-junction which doesn't let electrons in the n side to move to the p side. Otherwise, the pn-junction would be neutral and useless.

With the presence of sun light, the semiconductor absorbs photons according to its bandgap and dislodges electrons from the bonds creating extra mobile electrons and extra mobile holes called photocarriers. The extra mobile electron (the extra mobile hole) is also called minority charge carrier, since it was created inside the p-type (the n-type) semiconductor where there is an excess of holes (electrons) and as a result it will recombine again. However, if the minority charge carriers were generated very close to the electric field at the pn-junction or if they tend to flow into this region and manage to reach it before they recombine, the field acts as a driving force and steers the electrons to the n-side and the holes to the p-side. Connecting then both sides of the solar cell with a wire, the electrons from the n-side will travel round and recombine with the free holes in the p-side when they meet them again; returning the system to its starting condition. This flow of electrons at a certain direction caused by the field in the semiconductor results in the current. The electric field of

the cell results in the formation of a voltage. The current and the voltage give the power of the solar cell.

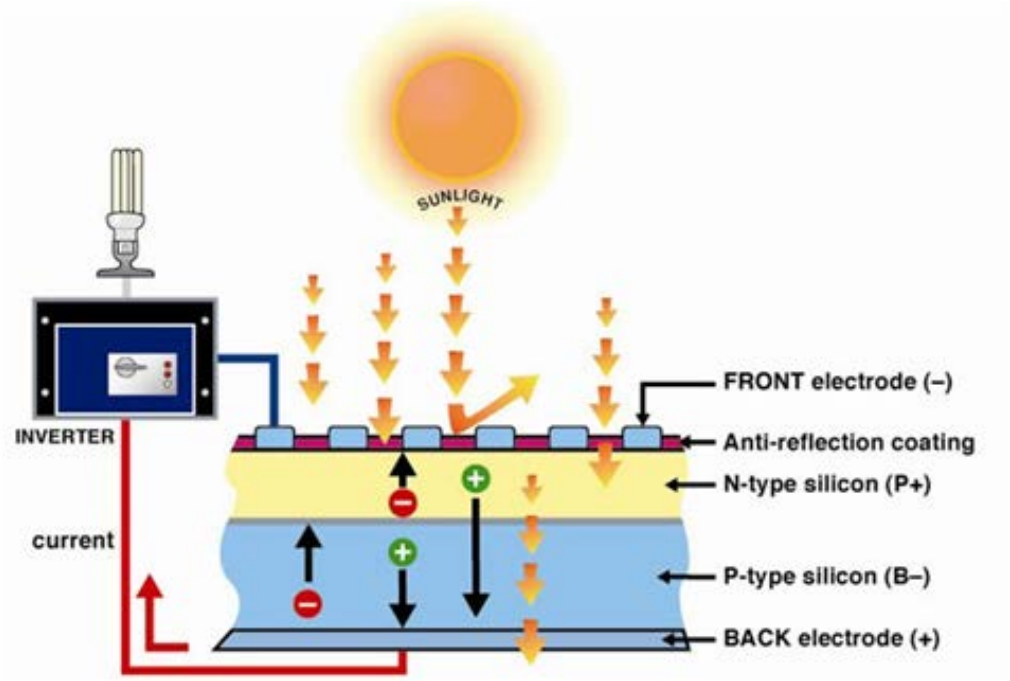

Fig. 1.1: *Solar cell structure and operation principles.*

As we discussed above, the photocarriers need to be collected from the pn-junction so as to result to the photocurrent. An important parameter for that is the diffusion length L_d, which is the average distance a charge carrier can move from point of generation until it recombines in a certain material. Fig. 1.2 shows the diffusion of the charge carrier from the region where photocarriers are generated to the pn-junction. Minority charge carriers generated far away more than the diffusion length from the pn-junction are not effectively collected, owing to bulk recombination (indicated by the asterisk). Therefore, solar cells with high collection efficiencies must have carrier diffusion lengths as the thickness of the absorbing material, a requirement that is most easily met for thin film cells.

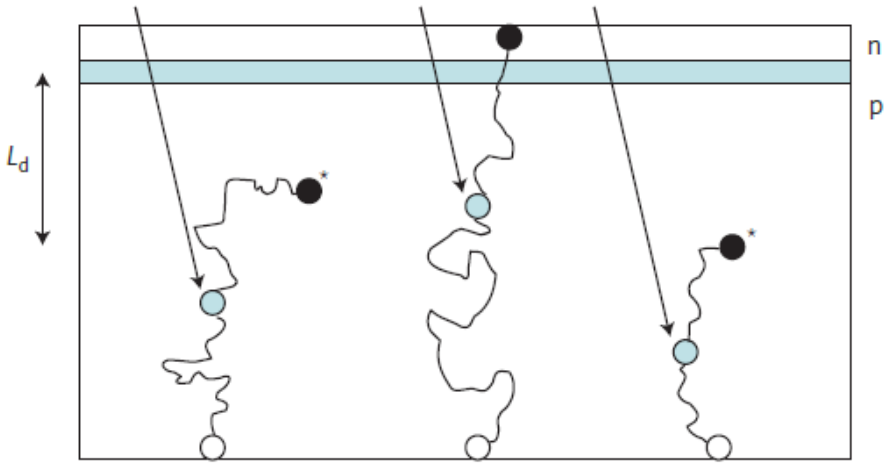

Fig. 1.2: *Minority charge carrier generation and collection by the pn-junction or bulk recombination (indicated by the asterisk)*[2]*.* L_d *is the diffusion length. The green filled circles correspond to the photo-generated electrons, the white circles to the photo-generated holes and the black circles indicate electron-hole recombination.*

Today's technology of solar cells is based on silicon semiconductor because Si is largely available and its energy bandgap is inside the range of the solar spectrum. Conventional solar cells are typically based on the more expensive crystalline silicon as it provides big diffusion lengths for the efficient collection of the photo-generated carriers. This helps to have bigger absorbing layers thicknesses which result to higher absorption at the expense though of the increased cost. Alternatively, thick but cheaper amorphous or microcrystalline silicon solar cells provide low collection efficiencies of photo-generated charge carriers. Therefore, the thickness of the absorbing material needs to be reduced while also the absorption must remain high.

Recently though, new advances in nanotechnology and material fabrication methods allow us to decrease the thickness of solar cells so as to avoid the recombination problem and reduce also the cost. One of the largest drawbacks of thin film silicon solar cells is the very small interaction time of the incoming wave with silicon, resulting to small absorption. Therefore, advances in the nanophotonics provide way to enhance the absorption using approaches like e.g. plasmonics. In this way, we can take advantage of the high local field values which are confined at metal-dielectric interfaces at the frequency region of their plasmon resonance and enhance the absorption.

If one looks in the literature, he will notice that several scientists studied the absorption of various media with potential use in solar cells. Yablonovitch[3] in 1981, established an analytical theory based on the ray optics principle for the maximum absorption limit, while other studies took into account the wave behavior of light and described new absorption limits through the local density of states (LDOS)[4].

When talking about solar cell geometries, there are two regimes that one needs to take into account: solar cells with big absorbing layer thicknesses where Yablonovitch theory holds, and solar cells in the nanophotonic regime, where dimensions are comparable with the wavelength scale.

Light trapping theory for solar cells with thick absorbing layers was firstly developed by Yablonovitch. Yablonovitch calculated the upper limit of absorption enhancement that was found to be $4n^2$ where n is the refractive index of the medium. The theory was derived from the ray optics perspective and exploited the effect of total internal reflection. This was achieved by roughening the air-silicon interface and this resulted to internal angular randomization, so that all the photonic states are filled equally. This theory stands for isotropic illumination and for collimated light beam with ergodic behavior (it forgets where and in which direction it came from) once the ray enters the medium. These situations are illustrated in Fig. 1.3(a) and (b) while Fig. 1.3(c) shows an example of a nonergodic geometry where the enhancement is small or zero.

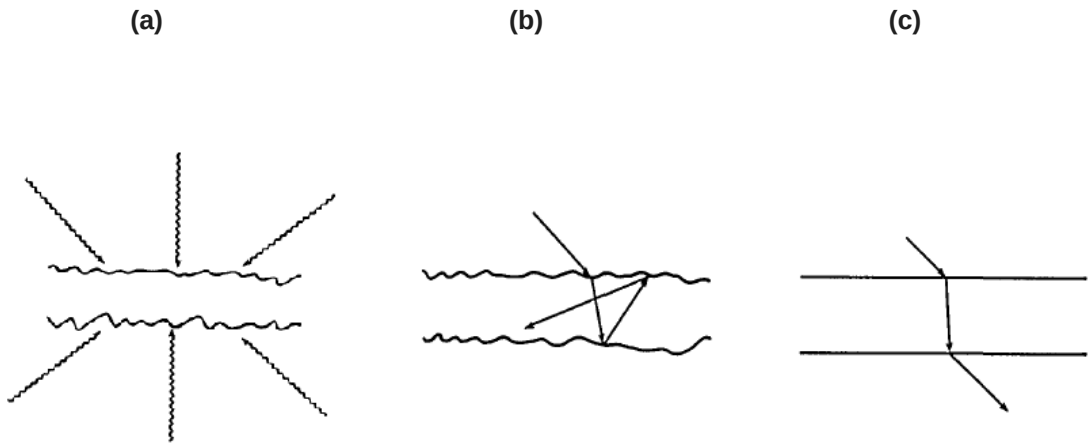

Fig. 1.3: *(**a**) Isotropic illumination on a textured sheet. (**b**) Internal angular randomization of a collimated light beam. (**c**) Nonergodic geometry leads to nonergodic behavior of the collimated light beam.*

In the nanophotonic regime with structures comparable with the wavelength scale, the critical point is that the optical density of modes per unit volume is affected by the wave optical effects and there is no longer an equal filling for all the photonic states. In addition, LDOS can be increased with new additional modes which are provided by the nanostructure from solving Maxwell equations because of the wave behavior of light.

As a result, if we choose appropriate coupling mechanisms like gratings, some photonic states can be enhanced at the expense of others, leading to absorption enhancement at specific desirable spectral regions which lead to enhanced photocurrents. This enhancement

can surpass the Yablonovitch limit, while, in the limit of very thick absorbing layers the enhancements lean towards the Yablonovitch upper limit.

Sheng et al.[5] stated that the grating may change the density of states leading to enhancement beyond $4n^2$ at a specific wavelength and angular range. Moreover, James M. Gee at al.[6] showed that the statistical limit can be exceeded over a limited spectral and angular range using carefully engineered photonic crystals. In this way, he managed to eliminate photonic states for all possible polarizations and angles over a spectral range (energy bandgap) and these states are moved to other portions of the spectrum where they can enhance absorption.

Solar cell performance can also be enhanced by exploiting the surface plasmon polariton (SPPs) modes. As explained by Schiff[7], statistical distribution of energy in the electromagnetic modes of the structure, which include the SPP modes at the metal-dielectric interface as well as the trapped waveguide modes in the film, can lead to $4n^2 + n\lambda/h$ enhancement, where h is the device thickness, in the absence of absorption inside the metal.

Callahan et al.[8] uses the density of states as a defining approach for understanding light absorption and he shows that an enhanced integrated local density of states is the fundamental criterion that determines whether light trapping structures can exceed the ray optics light trapping limit. Furthermore, Yu et al.[9] presented an analytical strategy based upon electromagnetic analysis showing that enhancement can exceed the conventional limit over a broader range of angles and frequencies than other studies, by reaching the single-mode regime of the absorbing film. The geometry of the structure provided that the mode exhibits a deep-subwavelength-scale electric field confinement inside a 5 nm ultra-thin absorbing layer in the absence of absorption inside the metallic back reflector.

Studies with such ultra-thin absorbing layers that achieve full benefit of the nanophotonics surpassing the Yablonovitch limit while being almost unaffected by the angles or the frequency range, raise another question regarding efficiency of solar cells: is it preferable to have ultra-thin absorbing layers that their absorption surpasses their Yablonovitch limit over the frequency spectrum? Or it is better to have thicker layers that do not surpass their Yablonovitch limit but have much higher absorption than the previous. In this work, the structures that are examined consist of thin absorbing layers for which the Yablonovitch limit is regarded as their theoretical limit, and the nanoparticles are used to redistribute the power at the wavelengths that matter.

Moreover, one should keep in mind that a plethora of factors affect the efficiency of solar cells, such as angular and spectral dependency of the resonances, the limiting factor of the unwanted parasitic absorption inside the metallic parts of the device, the carrier collection efficiency and of course the limitations by the existing fabrication technologies. Thus, optimal trade-offs need to be found having in mind the photocurrent efficiency over the solar spectrum.

1.2 Purpose of this study

Since, absorption is an essential parameter for solar cells efficiency, this study aims to enhance absorption in amorphous silicon thin film layers, by exploiting the principles of the plasmonic excitations. Both the Localized Surface Plasmon Resonances[10] (LSPRs) of metallic nanoparticles placed inside the cell and the excitation of the Surface Plasmon Polaritons[11] (SPPs) at the metal-dielectric interfaces using periodically nanostructured diffraction gratings, are examined. In addition, the absorption could also be enhanced by reducing reflection with resonant, dielectric nanostructures on top of the absorbing layer. The aim is to understand the effect of the nanoparticles shape, size, periodicity and position at the solar cell, upon these principles.

1.3 Organization of this thesis

In the present thesis, in order to understand the effect of the shape, size and periodicity of the metallic or dielectric nanoparticles upon the absorption of the solar cell, the chapters are divided regarding the position of the nanoparticles at the solar cell structure. In Chapter 2, the metal nanoparticles are periodically placed on top of the absorbing layer of the solar cell and the impact of their LSPRs is examined. In Chapter 3 the nanoparticles are placed at various positions inside the absorbing layer or at the top of the metallic back reflector, and both their LSPRs and the excitation of the SPPs are examined. In Chapter 4 deterministic, dielectric nanostructures are placed on top of the absorbing layer of the solar cell, and the optimum conditions (shape, size, period) for minimizing reflection are examined.

1.4 Simulation method

1.4.1 Software

Due to the complexity of the solar cell geometries that include metallic nanoparticles or other nanostructures for enhancing absorption, we use computational programs for electromagnetics for modelling the interaction of the electromagnetic fields with such complex geometries and solving these problems.

The electromagnetic simulation softwares used in this work are JCM[12] Suite and Computer Simulation Technology Studio Suite[13] (CST), which implement the Finite Element Method (FEM[14]), due to their speed and accuracy[15].

The frequency domain solver of the FEM is used in this work because it provides more accurate results and finer meshing based on the requirements for accuracy in a single frequency, or in broader range as long as the mesh size is valid in those frequency bands. This is important, since we deal with plasmonics and sharp resonances are resolved better.

1.4.2 Simulation

The simulation box of the structures that are examined is shown in Fig. 1.4.

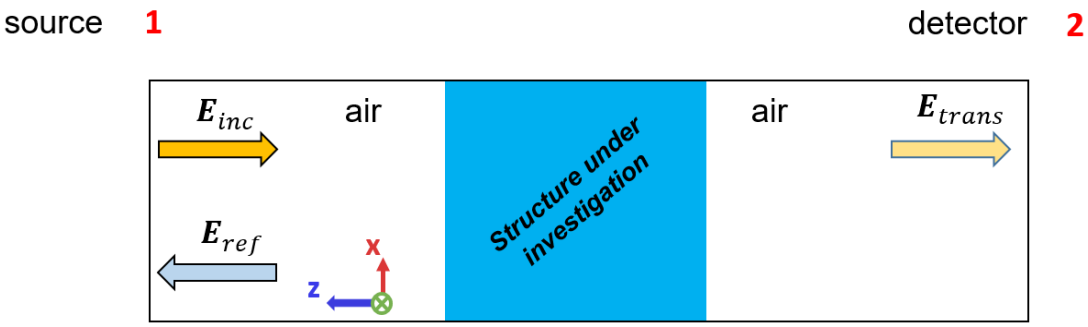

Fig. 1.4: *Simulation box of the structures that are examined.* E_{inc} *is the incident electric field and* E_{ref}, E_{trans} *are the calculated reflected and transmitted electric fields.*

Planewaves are launched from the source region and then the reflected (E_{ref}) and transmitted (E_{trans}) electric fields are calculated. The reflection coefficient is calculated from equation 1.1, and is given by the ratio of the calculated reflected electric field versus the incident electric field that we sent. Then the reflection (R) is defined as the reflection coefficient squared (equation 1.2). In the same way we calculate the transmission (T), (equations: 1.3, 1.4), and then we can find the total absorption (Abs) by equation 1.5.

$$S_{11} = \frac{\boldsymbol{E}_{refl}}{\boldsymbol{E}_{inc}} \qquad (1.1)$$

$$R = |S_{11}|^2 \qquad (1.2)$$

$$S_{21} = \frac{\boldsymbol{E}_{trans}}{\boldsymbol{E}_{inc}} \qquad (1.3)$$

$$T = |S_{21}|^2 \qquad (1.4)$$

$$Abs = 1 - T - R \qquad (1.5)$$

Moreover, for the structures that we examine in this work, we need also to find the absorption at different parts or materials of the solar cell. This is also possible since the simulation program calculates the electric field for each position of the structure so we can find the power that is lost at different parts or materials of the solar cell by integrating over the relevant volume.

2 Nanoparticles on top of the absorbing layer

2.1 Introduction

In this chapter metal nanoparticles are periodically placed on top of the absorbing layer of the solar cell. The aim is to examine the coupling properties of the metal nanoparticles with the absorbing layer, and their potential to increase the solar cell performance. For that we examine the influence of the nanoparticle shape, size and the periodicity on the absorption enhancement and the equivalent photocurrent generated by the solar cell. The absorption enhancement could be achieved either by exploiting the enhanced near-field amplitude of the metal nanostructures at their surface plasmon resonance, or their high scattering cross sections, hence providing coupling of light to the absorbing layer.

2.2 Localized Surface Plasmon Resonances (LSPRs)

Metal nanoparticles that support localized surface plasmon resonant (LSPR) modes[16] are important candidates for increasing absorption in thin film solar cells because they can effectively interact with light and confine it at their surfaces. LSPRs are collective resonant oscillations of conduction electrons of metallic nanoparticles that are excited by light. Their important characteristic is that they are associated with high near-field amplitudes and the strong scattering can play an important role in solar cells for light-coupling with the electromagnetic modes of the absorbing material.

The resulting scattering and absorption cross sections of metal nanoparticles can be calculated with numerical simulations or with analytical theories at simpler cases, like Mie theory[17] (spherical, no size bound nanoparticles) or Rayleigh theory[18] (spherical, small).

2.3 Photocurrent efficiency – Figure of merit

We begin our investigation by choosing the appropriate thicknesses for the absorbing layer in order to have efficient carrier collection. In this way, we can be safe enough regarding the electrical properties and the calculated theoretical carrier collection efficiency of the solar cell.

Fig. 2.1(a) shows the maximum theoretical absorption, calculated by equation[19] 2.1 which was derived by the Yablonovitch theory[20,21,22], assuming perfect light trapping and zero reflection, for an absorbing layer with 400 nm thickness and a layer with 1.5 μm thickness for comparison, along with their equivalent integrated theoretical photocurrents (Fig. 2.1(b)). The thicknesses in this work will be 400 nm and less, as studies[23,24] for amorphous silicon suggest for efficient light harvesting in applications like photovoltaics.

The main active material for the absorbing layer of the solar cells in this work is amorphous hydrogenated silicon (a-Si:H), [the dielectric function is shown in Fig. 2.2(a)].

$$A_{Yablonovitch} = 1 - \frac{1}{1 + 4n^2 ad} \qquad (2.1)$$

In equation 2.1, n is the real part of the refractive index, d is the thickness of the absorbing layer and α is its absorption coefficient.

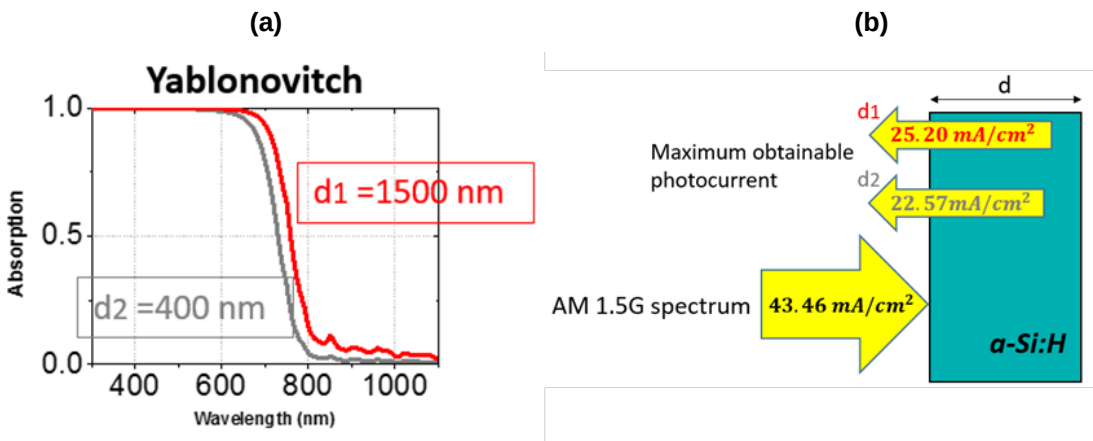

Fig. 2.1: *(**a**) Maximum theoretical absorption for a-Si:H layers with thicknesses of 400 and 1500 nm, calculated by Yablonovitch theory (assuming perfect light trapping and zero reflection at the top), and (**b**) their equivalent integrated theoretical photocurrents.*

From the absorption in the active layer one can calculate the equivalent photocurrent assuming that each absorbed photon results in an electron-hole pair, which is effectively collected (unity internal photocarrier efficiency). This is a good approximation since the structures that we examine have thicknesses of 400 nm and less, thus it is smaller than the thicknesses suggested for efficient photo-generated carrier collection[23,24]. The photocurrent J_{equiv} is calculated by equation 2.2:

$$J_{equiv} = q_0 \int A(\lambda)\Phi_{AM1.5G}(\lambda)d\lambda \qquad (2.2)$$

where q_0 is the electron charge, $A(\lambda)$ is the absorption, and $\Phi_{AM1.5G}(\lambda)$ is the photon flux density of the AM 1.5 solar spectrum. J_{equiv} is used as a figure of merit (FOM) to compare the performance of the structures examined, by substituting the $A(\lambda)$ with the calculated absorption for each structure.

2.4 Results and discussion

2.4.1 Materials and the structure

Metal nanoparticles have a scattering cross-section much larger than their geometrical cross-section near the LSPR wavelengths. Moreover, for metal nanoparticles placed on top of a high index active layer like silicon, the forward scattering inside silicon can dominate over backward scattering. More than 90% of the incident light can be scattered into the silicon substrate due to the abundance of optical modes available[25]. As a result, more light can be coupled to the electromagnetic modes of the absorbing layer, leading to optical path length enhancements, decreasing as well the reflection that doesn't let light get inside the silicon.

However, as we are going to see in the following results, many other parameters affect light-trapping. Therefore, a careful analysis is required when we want to enhance absorption with metal nanoparticles on top of the absorbing layer, or else, this may even lead to negative photocurrent enhancements.

Before moving to the results, we provide the details about the structures, the materials and the simulation method. The FEM solvers of JCM and CST were used, with periodic boundary conditions, in order to examine periodically placed metallic nanoparticles on top of the absorbing layer, with a metallic back reflector at the back part of the solar cell structure. The absorbing material is a-Si:H with a dielectric function shown in Fig. 2.2(a) obtained from experimental data by Matthias Zilk Jena[26], and the metal nanoparticles and the back reflector consist of silver (Ag) with a dielectric function shown in Fig. 2.2(b) obtained from Palik[27].

(a) **(b)**

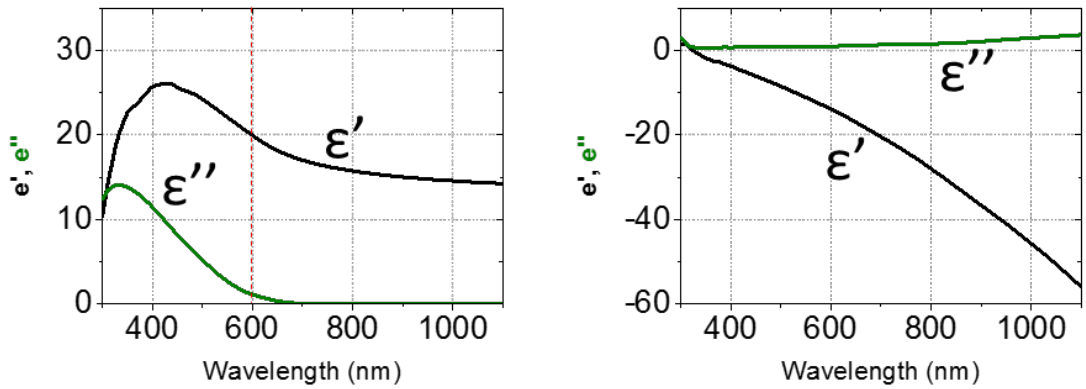

Fig. 2.2: *(**a**) Dielectric function of a-Si:H. The red dotted line distinguishes the absorbing, non-absorbing region of a-Si:H. (**b**) Dielectric function of Ag.*

As one can see from the imaginary part of the dielectric function of a-Si:H, the absorption edge of the material –where the material starts to absorb poorly- is between 600 to 700 nm. Consequently, the plasmonic resonances should be tuned to work better for wavelengths from 400 to 700 nm and especially at wavelengths where the sun radiates most of its power.

The typical structure of the unit cell studied in this work is shown in Fig. 2.3. The nanoparticles on top of silicon have 2D periodicity, in order their plasmonic resonances to be equally excited both for transverse magnetic field (TM) to the plane of incidence and for transverse electric field (TE) polarization for normal incidence.

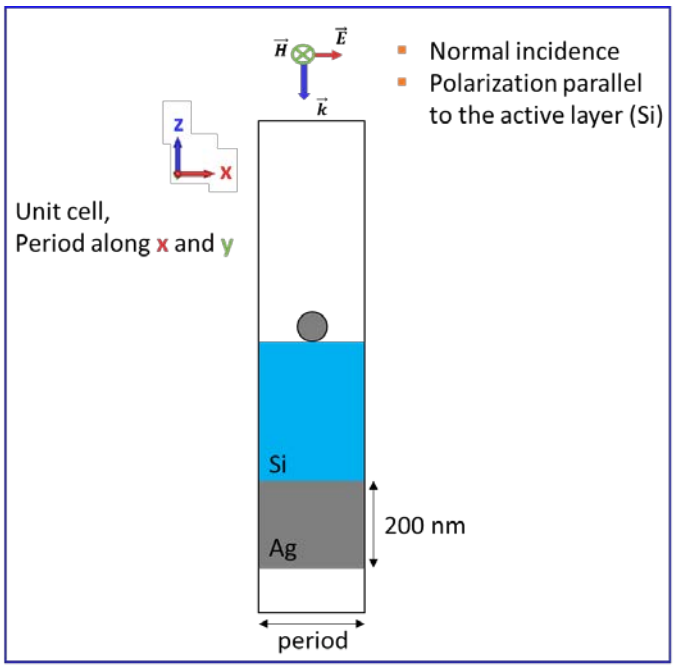

Fig. 2.3: *Unit cell of the typical structure examined. The structure consists of a silver back reflector with a thickness of 200nm, and periodically placed silver*

nanoparticles of various shapes and sizes on top of the Si absorbing layer.

2.4.2 *Light trapping performance of Ag nanoparticles with different shapes*

After optimization in respect to the wavelengths where the sun radiates most of its power, the best results were given by spheres. It was found that the period at which the spherical nanoparticles with a diameter of 100 nm are arranged, should be 185 nm. It is noted that large periods dilute the impact of the metal nanoparticles, while smaller periods lead to strong inter-particle coupling, where the non-radiative losses are increased[28].

The second column of Table 2.1 shows the photocurrent enhancements (compared with a bare silicon slab on a silver back reflector), after optimization for each nanostructure on top of the silicon layer in column one, for normal incidence and polarization parallel to silicon. The third column shows the equivalent photocurrent of the absorbed fraction of light inside the a-Si:H, and the fourth column the ratio % of the absorbed photocurrent versus the photocurrent calculated from the theoretical absorption limit.

Table 2.1| Light Trapping Performance.

Nanostructure	J_{equiv} Enhancement factor over un-patterned cell	J_{equiv} (mA cm^{-2})	Ratio: J_{equiv} / J_{Yablo} %
Spheres	1.294	13.0	57.4
Cylinders	1.048	10.5	46.5
Hemispheres	1.008	10.1	44.7

The equivalent photocurrent J_{equiv} was calculated for the wavelength range between 300 and 1,100 nm.

As mentioned above, the highest enhancement was found for spheres with a diameter of 100 nm and a period of 185 nm. The highest enhancements for cylinders with the same diameter, a height of 50 nm and a period of 400 nm where almost zero. Results in Table 2.1 show that spheres which possess a smaller surface contact area than cylinders or hemispheres, trap light more efficiently inside the silicon substrate. In addition, we observe that the ratio of the absorbed photocurrent compared with the theoretical limit, indicates poor enhancements well below the theoretical limit (fourth column in Table 2.1). These results are going to be explained in the next subsections.

2.4.3 *Absorption enhancement dependence on the surface contact area of the metallic nanoparticle with the active layer*

It is well-known that as the particle size or the refractive index of the surrounding medium increases, except for dipoles also higher order modes (quadrupoles, octupoles, etc.) appear

in the optical part of the spectrum; resonances red shift and broaden, due to increased retardation effects[29] across the particle. Due to the presence though of the high-index absorbing layer below the nanoparticles, the symmetry of the system is broken. The electromagnetic field induces a charge polarization on the particle which in turn causes a charge distribution on the absorbing layer that affects the nanoparticle and its proper modes.

For nanocylinders or hemispheres this phenomenon is more pronounced since they are more exposed to the change of the environment, in comparison to the spheres. Fig. 2.4 [(a),(b)] show the Mie resonances of an Ag sphere with a diameter of 100 nm isolated in air [in (a)] and the Mie resonances of an Ag cylinder in air with the same diameter and a height of 50 nm [in (b)]. “D” symbolizes the dipole mode of the nanoparticle and “Q” symbolizes the quadrupole mode.

Fig. 2.4 (c) shows that for normal incidence and polarization parallel to the Si absorbing layer (see Fig. 2.3), arrays of silver spheres [with the same diameter as in Fig. 2.4(a)] with a period of 185 nm, experience a weak coupling with the silicon layer, because of their small contact surface area with silicon. Consequently, their dipole Mie resonance is almost unaffected by the high index Si layer so it stays almost at the same wavelengths as the dipole mode in the case of the nanoparticle that is isolated in air [shown in Fig. 2.4(a)]. As a result, an important fraction of light is scattered inside the high-index absorbing layer, for wavelengths ~450-600 nm, and the absorption is enhanced. The mechanism for the forward scattering results from the higher density of states into the high index silicon.

On the other hand, as shown in Fig. 2.4(d), plasmon resonances of silver cylinders (with the same period), which have a large surface contact area with silicon compared to the spheres, are more exposed to the high index silicon and their dominant dipole resonance shifts to higher wavelengths where silicon does not absorb.

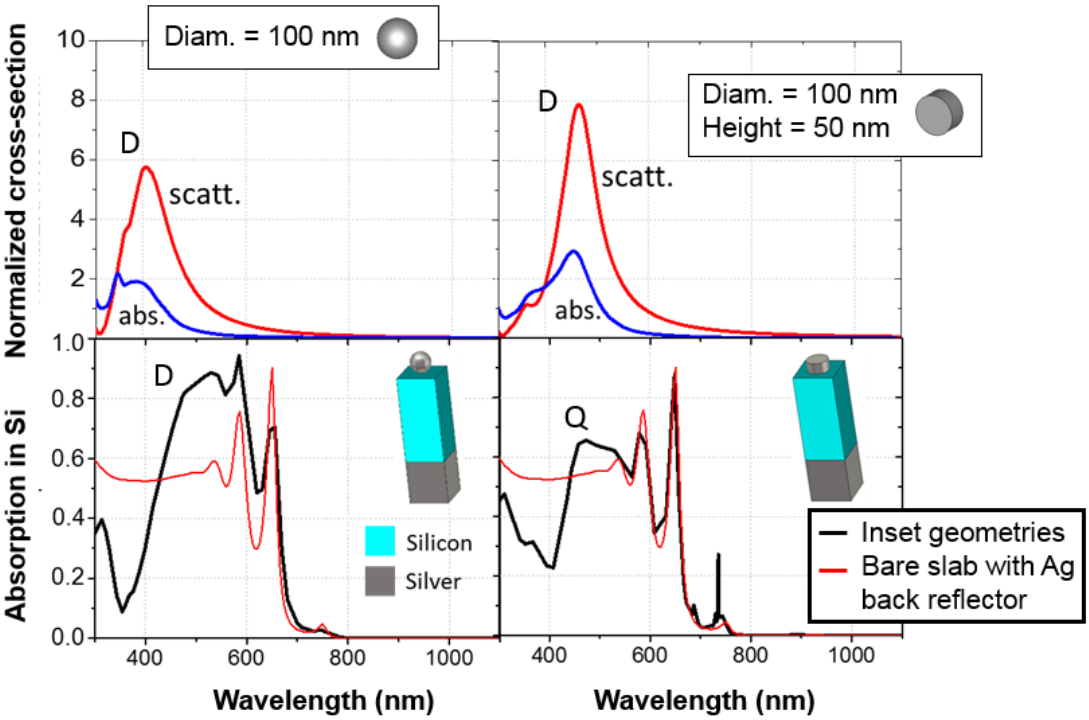

Fig. 2.4: [*(**a**)-(**b**)] Absorption (blue line) and scattering (red line) cross-sections of an isolated silver sphere with a diameter of 100 nm, and a silver cylinder with the same diameter, and a height of 50 nm. The cross-sections are normalized with the particles cross-section. Solutions are obtained from Mie theory for nanoparticles in air.* [*(**c**)-(**d**)] Absorption inside the silicon layer, for structures with periodically placed nanoparticles on top (black lines). The red lines show the absorption inside silicon for the same structure without the metal nanoparticles. Insets: the unit cell of the geometry considered. "D" symbolizes the dipole mode of the nanoparticle and "Q" symbolizes the quadrupole mode.*

The small absorption enhancement compared with the bare silicon structure shown for the cylinder nanoparticles at 465 nm [Fig. 2.4(d)] is an example of the asymmetric environment that scattering nanoparticles exhibit. Although the dipole resonance of the cylinder has moved to higher wavelengths compared with the Mie resonance solution in air [shown in Fig. 2.4(b) at ~463 nm], the quadrupole Mie resonance [small shoulder at ~363 nm, shown in Fig. 2.4(b)] is almost unaffected by the high index substrate and it redshifts slightly. The reason of this behavior of the plasmonic resonances is shown in Fig. 2.5, where the field distribution of the cylinder at the wavelengths of resonance for both the nanoparticle placed in air and on the silicon substrate is depicted. The following results are in good agreement with the observation of Hagglund et al.[30] and Spineli et al.[31].

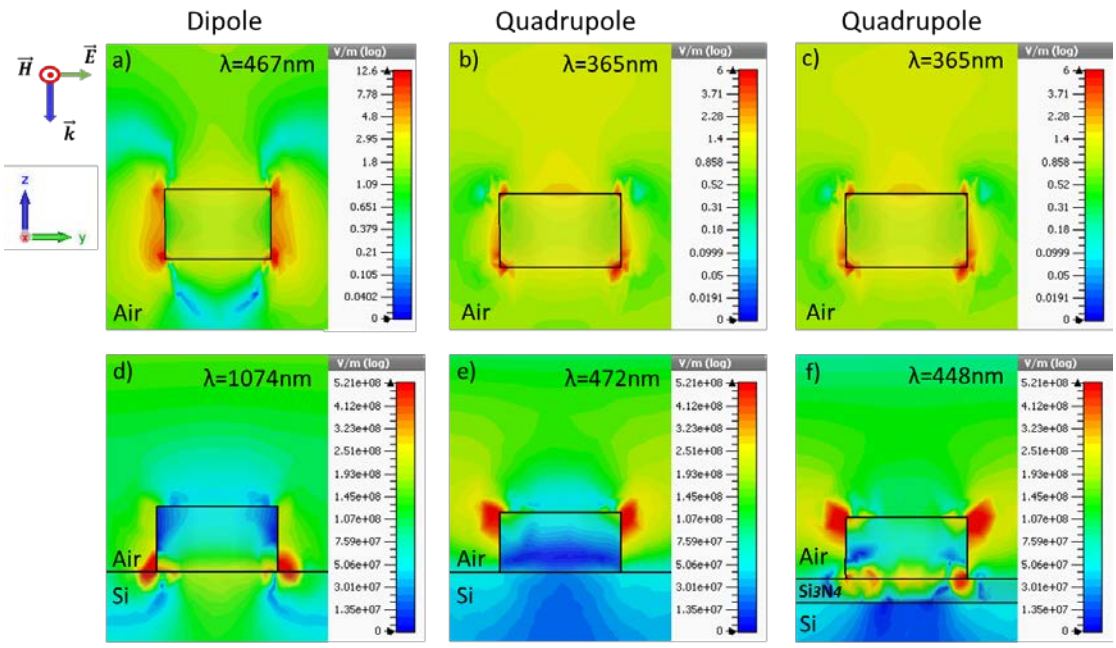

Fig. 2.5: *Amplitude of the electric field (y component parallel to the substrate) for polarization parallel to the substrate at the y axis. (**a**) Shows the dipole resonance of*

*an isolated cylinder in air, and (**b**)-(**c**) the quadrupole resonance of an isolated cylinder in air. It is noted that (b) and (c) show the same picture for illustration reasons and easier comparison with (d), (e), and (f). (**d**) The dipole resonance shown in (a) has shifted at the infrared, since its field distribution is modified and exists closer to the high index substrate. (**e**) The quadrupole distribution for an isolated sphere in air shown in (b) behaves as a dipole-like resonance at the particle-air interface when the cylinder is placed on top of silicon, thus, it doesn't redshift significantly. (**f**) When a Si_3N_4 (ε=4) intermediate layer is added, the field distribution of the resonance resembles more the quadrupole resonance of the isolated cylinder in air shown in (c).*

As one can see, the dipole resonance of the cylinder in air becomes a dipole-like field distribution exactly at the interface with silicon, thus, it is more exposed to the change of the refractive index of the silicon and consequently it shifts at the infrared [Fig. 2.5(a) and (d)]. On the other hand, the quadrupole resonance of the cylinder in air behaves as a dipole-like resonance which is located closer to air [Fig. 2.5(b) and (e)], and as a result its character is mostly unaffected by the silicon and it doesn't redshift significantly. Moreover, Fig. 2.5(c) and (f) show how sensitive is the cylinder to its environment. With the input of an intermediate, very thin (20 nm thickness), Si_3N_4 layer with a refractive index closer to air (ε=4), between the silicon substrate and the cylinder, the resonance takes again a field distribution closer to the case of the cylinder in air.

Furthermore, as it was shown in Table 2.1, it seems that the ideal shape for the nanoparticles is spheres because their plasmon resonances are mostly unaffected by the silicon layer and therefore located at lower wavelengths were silicon absorbs more. In addition, the dominant dipole resonance of spheres decays slower[32] (r^{-2}, r^{-3}) than other modes (e.g. quadrupole ~ r^{-5}) enhancing in this way the near-field coupling with the silicon layer.

However, the shape itself is not so important compared with the proximity and coupling with the active layer. Fig. 2.6 shows how much affected is the cylinder if we lift it 10 nm from the Si layer, in comparison with the lifted sphere which is almost unaffected. The lifted cylinder shows a similar behavior with the sphere because the dipole plasmon resonance blueshifts. As the contact surface area with silicon decreases the nanoparticles are more decoupled from it and their dominant dipole resonance is located at lower wavelengths and therefore it radiates light inside silicon at the wavelengths where silicon absorbs.

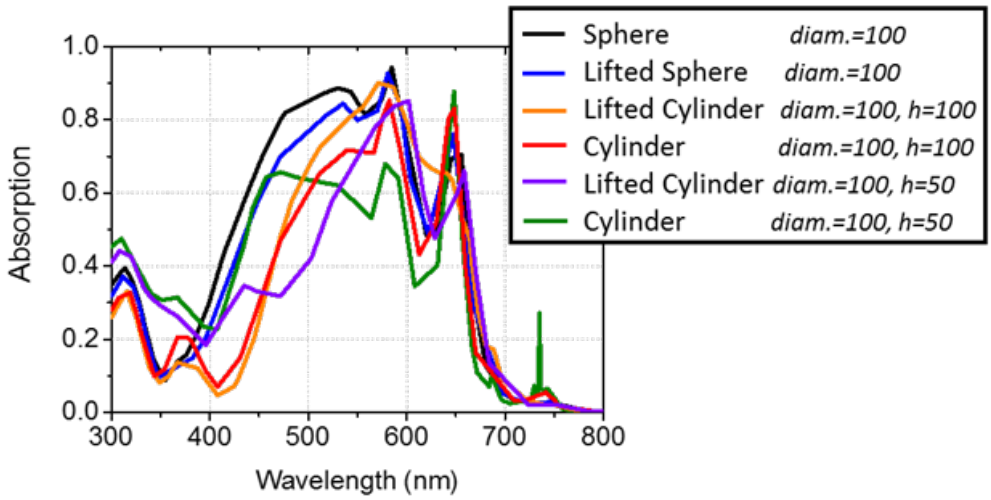

Fig. 2.6: *Absorption in silicon as a function of wavelength for structures with Silver nanoparticles (cylinders, spheres) on top of the silicon absorbing layer like the inset of Fig. 2.4. Diam. is the diameter of the nanoparticles and h is the height of cylinders.*

In practice though, lifting nanoparticles is not possible and doing so with an intermediate spacer comes at the expense of the reduced near-field coupling. However, the main problem, as shown in the Fig. 2.4(c) and (d), is the reduction of the absorption below the resonant wavelength and their subsequent negative effect to the photocurrent as it is explained at the next subsection.

2.4.4 *Absorption reduction at the wavelengths below the Mie resonances*

The absorption enhancements observed at certain wavelengths for spheres [Fig. 2.4(c)] are due to the scattering of light inside Si which has a very high density of optical modes. Though, the absorption inside Si was always reduced at the left of the plasmonic resonances (at lower wavelengths), and this had detrimental effects to the overall absorption efficiency of the structure. Thus, the metal nanoparticles can enhance the photocurrent, but also if the structure is not designed properly, they can even decrease it.

The reason for this phenomenon is the destructive interference between the scattered light from the nanoparticle and incident light, at wavelengths below the resonance. In Fig. 2.7(a), we can see that for wavelengths lower than 575 nm, the absorption inside the metallic spheres is increased, or the light is reflected, while for higher wavelengths than 575 nm the light is transmitted and couples with the active layer.

In order to have some insight to this phenomenon, we consider as a good approximation[33] that silver spheres are small (diameter =100 nm) compared to the wavelengths of the incident light, so as to use the quasistatic theory of the dipole radiation from a spherical nanoparticle.

When an electromagnetic wave is incident on a spherical particle with a dielectric constant ε_p in a surrounding medium with ε_0, it induces a dipolar oscillation at the particle, polarized at the direction of the incident electric field, $\boldsymbol{E}_0(t)$. The dipole moment, $\boldsymbol{p}$, induced in the spherical particle is given by the equation 2.3, where α is the polarizability of the particle given by the equation 2.4, and r is the radius of the sphere.

$$\boldsymbol{p} = \alpha \boldsymbol{E}_0 \qquad (2.3)$$

$$\alpha = 4\pi r^3 \left(\frac{\varepsilon_p - \varepsilon_0}{\varepsilon_p + 2\varepsilon_0} \right) \qquad (2.4)$$

As one can see, for a metallic sphere where ε_p is complex and wavelength dependent, α is a complex number and exhibits a wavelength dependence, i.e. the field radiated by the induced dipole, will have a wavelength dependent and non-zero phase from the incident field. The plot of the magnitude, $|\alpha|$, and phase φ (of the polarizability $\alpha = |\alpha| e^{i\varphi}$ normalized to the volume of the sphere: $\frac{4}{3}\pi r^3$) versus the wavelength is shown in Fig. 2.7(b).

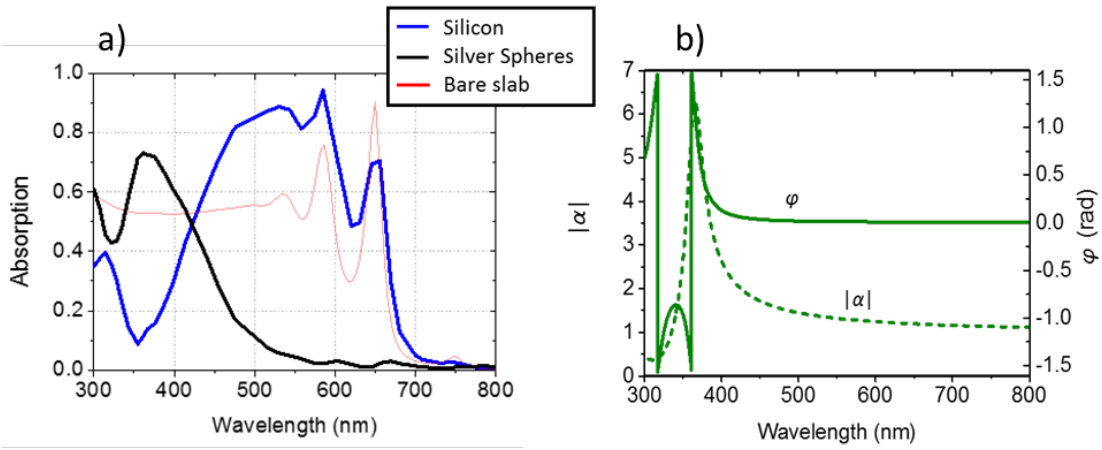

Fig. 2.7: *(**a**) Absorption in silver spheres (black line) on top of silicon with a silver back reflector. Absorption in silicon (blue line), and absorption in silicon for a slab without the spheres on top (red). (**b**) Magnitude, $|\alpha|$, and phase φ (of the polarizability $\alpha = |\alpha| e^{i\varphi}$ normalized to the volume of the sphere $\frac{4}{3}\pi r^3$) versus the wavelength.*

It is clearly seen that for wavelengths below 360 nm, α has a negative phase, which leads to destructive interference between the forward scattered and the incident field, resulting to reduction of the field which is transmitted inside silicon. As a result, light is almost not

transmitted at all for certain wavelengths below the resonance. The incident radiation is either reflected or absorbed by the metallic nanoparticles and the second becomes more and more robust when the periodicity gets smaller. On the other hand, for wavelengths higher than 400 nm the phase of α is almost zero, and the incident and transmitted fields are almost in phase. These results are in good agreement with the case of spheres with 100 nm diameter, on top of the silicon substrate [Fig. 2.7(a)].

The above mentioned phenomenon plays an important role for the efficiency of solar cells and the geometry and the shape of the nanoparticles should be carefully chosen, as to increase the light transmitted into the Si active layer.

In order to examine the impact of the nanoparticles shape regarding this phenomenon, we calculated the normalized transmission given by the nanoparticles on top of the absorbing layer, compared with the bare silicon layers. For the calculations (geometry shown in the inset of Fig. 2.8) we used the frequency domain solver (FEM) with periodic boundary conditions and perfectly matched layer (PML) boundaries at the bottom side of the silicon layer, assuming semi-infinite silicon. The total transmission of the structure included both the transmission at the bottom part (see the geometry inset in Fig. 2.8) and the absorption inside silicon.

Fig. 2.8 shows that arrays of spheres provide better transmission factors inside the active layer because their dominant dipole resonance is located at lower wavelengths. In contrast, nanoparticles with higher surface contact area with the high index silicon like the cylinders, exhibit redshifted plasmonic resonances and cover a wider spectrum, facilitating in this way the broadening of the negative phenomenon of the destructive interference between the forward scattered and the incident field below the resonant wavelengths that affects negatively the overall absorption enhancement. The huge decrease in the normalized transmission at almost 1040 nm is attributed to the shifted at the infrared dipole resonance of the cylinders. Moreover, the first dip of the blue line corresponds to the quadrupole resonance of the cylinders, and the first dip of the green line corresponds to the dipole resonance of the spheres.

Our findings are in good agreement with the results of Spineli et al. with the addition that the transmission factors calculated in this work are severely decreased, reaching values even close to zero (in comparison with Spineli's work, that the lowest transmission factors where ~0.9), owing to the strong absorption inside the silver nanoparticles, due to strong interparticle-coupling between the periodically placed nanoparticles that suppresses the radiative scattering. Increasing though the period leads to the weakened impact of the Mie resonances of the diluted nanoparticles and thus to worse results.

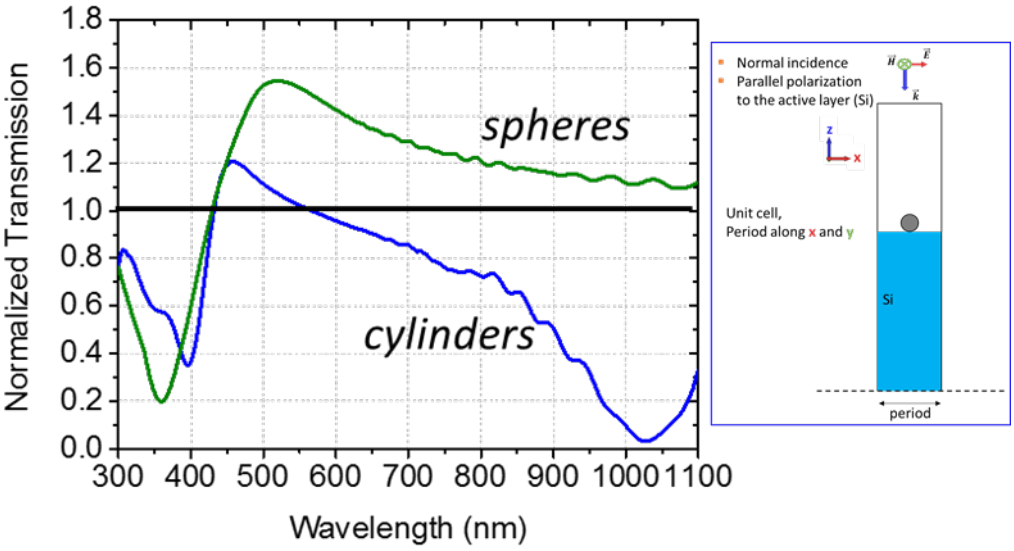

Fig. 2.8: *Normalized transmission compared with a bare slab without silver nanoparticles on top. The first dip of the green line (~350nm) corresponds to the dipole resonance of the spheres, and of the blue line (~400nm) to the quadrupole resonance of the cylinders. The second dip of the blue line (~1040nm) corresponds to the dipole resonance of the cylinders. The geometry considered for the calculations is shown in the inset at the right.*

The next step was to put intermediate layers with lower refractive index than silicon between the silicon layer and the cylinders and check the influence on the in-coupling of the incident radiation within the silicon layer. Using lower refractive index spacers is a well-known technique that shifts the plasmonic resonances to lower wavelengths where silicon absorbs more. The mechanism of this technique is the reduction of the effective index in the region surrounding the particle, at the expense though of the reduced near field coupling between the particle and the silicon.

Fig. 2.9 shows the normalized transmission, as a function of the wavelength, for arrays of cylinder nanoparticles on top of the Si_3N_4 (ε=4) dielectric spacers with a varying thickness, t, separating the nanoparticles from the Si layer. The calculation method was the same as in Fig. 2.8, and the normalized transmission was found by comparing the transmission of each structure, with the transmission of the same structure, with the corresponding intermediate spacer, but without the silver nanoparticle on top.

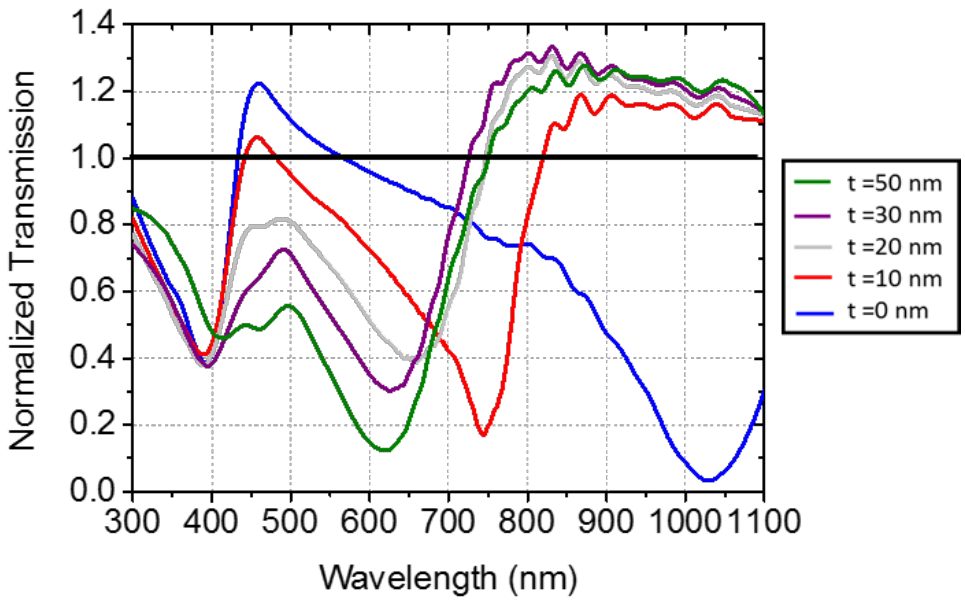

Fig. 2.9: *Normalized transmission caused by silver cylinders on top of Si_3N_4 (ε=4) intermediate layers between the silicon layer and the cylinders. The thickness of the intermediate layer is defined as t. The transmission of each structure is normalized with the transmission of the same structure, with the corresponding intermediate spacer, but without the silver nanoparticle on top.*

One can see that as we increase the thickness of the Si_3N_4 layer from 10 to 50 nm, the transmission enhancements (~750-1100 nm) blueshift. The dips at the left of the transmission enhancements are associated with the destructive interference between the forward scattered and the incident field for the wavelengths below the plasmonic resonances. It is clearly seen that for wavelengths between ~500-750 nm there is a strong reduction in the transmission that reaches values even close to zero for *t*=50nm.

When the structure is without the intermediate spacer, the plasmonic resonance is shifted to the infrared since it is more exposed to the high index substrate, therefore, the dip associated with the wavelengths below the plasmonic resonance is at higher wavelengths (~1040 nm) than for the structures with the spacers. The peaks shown at ~490 nm correspond to the quadrupole mode of the cylinder. As we discussed in subsection 2.4.3, because of its higher field values at the metallic-air surface, it remains unaffected by the high index substrate and it doesn't redshift to higher wavelengths. In addition, as the thickness of the spacer gets smaller, the quadrupole resonance behaves more as a dipole-like field distribution, because of the broken symmetry induced by the substrate, and as a result it radiates more efficiently (r^{-2}, r^{-3} vs r^{-5}) reaching 1.2 transmission enhancement when the structure is without the spacer.

2.5 Conclusions

In summary, we have studied the influence of the shape of the metallic nanoparticle arrays on top of a Si layer, on the absorption enhancements by the Si layer. It was shown that spheres give better results compared to nanoparticles with larger contact surface area with silicon like cylinders or hemispheres, due to their unaffected dominant dipole resonances at lower wavelengths were silicon absorbs. In addition, the shifted dipole resonances of the cylinders at the infrared caused a reduction in the light that is transmitted inside silicon for wavelengths of 550 nm and then (Fig. 2.8) due to the broadening of the effect of the destructive interference between the forward scattered and the incident field for the wavelengths below their plasmonic resonances (Fig 2.7). Moreover, higher-order modes provide reduced coupling into the silicon substrate than dipole modes, because the field around the particle decays faster. For the reasons above, and in addition to the more convenient experimental nano-fabrication, spheres are considered to have the ideal shape when targeting absorption enhancements for solar cell with nanoparticles on top of the absorbing layer. Finally, because of the reduction in transmission inside the silicon substrate caused by the destructive interferences between the incident and the scattered light, and the aggravation of this effect owing to strong inter-particle coupling of the periodically placed nanoparticles, the overall enhancements were below the theoretical upper limit.

3 Nanoparticles inside the absorbing layer and on the back reflector

3.1 Introduction

The most prevalent bulk material for solar cells is crystalline silicon (c-Si), and especially monocrystalline silicon (mono-Si), which is more efficient but quite expensive, making thus the photovoltaics industry to turn its attention mostly to thin-film cells (of sub- to few micron

thickness), requiring less material, and to amorphous or microcrystalline Si which is less expensive. One of the largest drawbacks though of thin film silicon solar cells is the very small interaction time of the incoming wave with silicon, resulting to small absorption. A possible approach to increase this absorption is to place metal nanostructures inside the absorbing layer of the solar cells and exploit the enhanced scattering and high local field values caused by such nanostructures due to the excitation of surface plasmons.

The aim of this chapter is to analyze the effects of surface plasmons on the absorption properties and thus the efficiency of thin film cells and to explore how surface plasmon generating structures can be exploited to increase solar cell efficiency in silicon solar cells. This is done by studying two approaches:

a) Exploiting the LSPR of the metal nanostructures. In this approach the nanostructures exhibit enhanced scattering and high local fields. Metal nanostructures are periodically placed either at the solar-cell back reflector or in other places inside the absorbing layer of the cell. We investigated metal nanostructures of different shapes and sizes, different periodicities and different locations in the unit cell in order to find the optimum conditions for maximizing the cell absorption.

b) Using the nanostructures as a grating to excite the surface plasmon polaritons[34] (SPPs) of the Si-metal (back-reflector) interface; such SPPs are also associated with high local fields and therefore can promise also high absorption.

3.2 Results and discussion

3.2.1 Exploiting Localized Surface Plasmons inside Silicon

In order to avoid the destructive interference effects when the nanoparticles are placed on top of the absorbing layer as shown in Chapter 2 and the consequent poor absorption enhancements, now the metallic nanoparticles are placed inside the Silicon, at various positions. The disadvantage of this approach is that the antireflection properties are lost. (The metallic nanoparticles on top, at the wavelengths of their plasmonic resonance, exhibit big scattering cross-sections redirecting in this way the incident light inside the active layer.) Therefore, with the nanoparticles inside silicon, we must use antireflection coatings on the top part of the structures to achieve antireflection.

Fig. 3.1(a) shows how much distance light propagates until it is absorbed inside an a-Si:H layer. As one can see, for wavelengths above 600 nm, for an a-Si:H layer of 400 nm thickness the radiation impinging on it can be absorbed with a single pass. So, the radiation that is lost from a bare slab with Ag back reflector below 600 nm wavelength [red transparent line in Fig. 3.1(b)], is due to the reflection from silicon and the reflection is more than 40% on average for these wavelengths. Therefore, in order to take full advantage of the metallic nanoparticles, the radiation that reaches them should be the maximum possible.

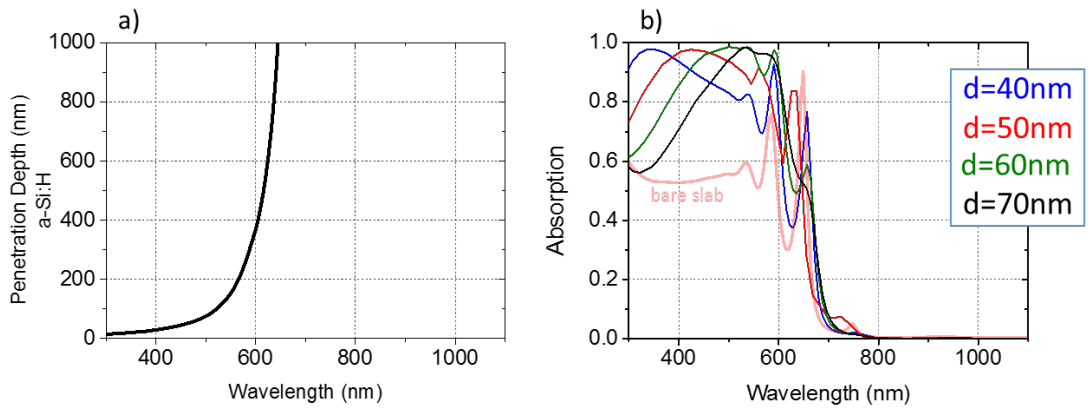

Fig. 3.1: *(**a**) Penetration depth for a-Si:H, showing how far into a material light of a particular wavelength can penetrate before it is absorbed. (**b**) Absorption inside silicon with 400 nm thickness, on top of an Ag back reflector, for different thicknesses of a Si_3N_4 (with ε=4) antireflection coating on top of the silicon.*

Fig. 3.1(b) shows that by reducing the reflection coefficient[35] with a simple antireflection (AR) coating (Si_3N_4 with ε=4) on a 400nm thick Si cell with an Ag back reflector, the absorption reaches 1 for certain wavelengths depending on its thickness.

Although the AR coatings provide enhanced absorption inside silicon by reducing reflection, the incident light cannot couple efficiently into the EM modes of the silicon, because there is refraction but not scattering to couple with the EM modes of the slab, and this is very important for thin film solar cells. So, we combine AR coatings, which suppress reflection on top of the solar cell, with metallic nanoparticles at different places and different periodicities inside silicon, in order to take advantage of their scattering cross-sections and the enhanced field localized on their surface at the LSPR.

The contributions to the absorption enhancement inside the absorbing layer of the thin film solar cell, from both the metal nanoparticles and the AR coating were examined individually and compared. Also, different thicknesses (50-400 nm) of the absorbing layer were examined.

It is shown that metallic nanoparticles without the AR coating lead to poor enhancements, compared with the AR coating alone, while indeed their combination exceeds the enhancements of either of these structures individually. However, it was found that the enhancements come mostly from the coupling of the incident light with the waveguide modes[36] of the Si slab which are excited by the periodicity of the nanoparticles that phase-matches with the modes of the slab, rather than from the LSPRs, in agreement with other studies for amorphous silicon solar cells[37].

3.2.2 Exploiting LSPR of metal nanoparticles

We examined nanostructures of different shapes (sphere, hemisphere, cylinder, cylindrical pillar, cube), both 2-dimensional periodicity and one-dimensional periodicity (e.g. stripes), and the nanoparticles are placed either on top of the metallic back-reflector or inside the Si layer in different depths:

a) Structures with *2D* periodicity which were investigated:
   i. *Period*: 25-400 nm
   ii. *Si layer thickness (d)*: 50-400 nm
   iii. *Positions in cell*: Top of back-reflector, at *d/4* depth (from bottom of a:Si), at *d/2* depth, at *3d/4* depth
b) Structures with *1D* periodicity which were investigated:
   i. *Period*: 25-3000 nm
   ii. *Si layer thickness (d)*: 50-400 nm
   iii. *Positions in cell*: Top of back-reflector, at *d/4* depth (from bottom of a:Si), at *d/2* depth, at *3d/4* depth

Table 3.1 and Table 3.2 below present the nanostructures which gave the most promising results regarding the highest theoretical photocurrents, while the structures that gave the highest photocurrent enhancements (compared with their reference structure) are going to be discussed in detail later. For all the cases of Table 3.1 and 3.2, the highest photocurrents were given for the silicon layer with the biggest thickness (400 nm).

As was mentioned earlier, to avoid back reflection from the top Si surface exploiting thus more the presence of the nanostructures and illustrating more clearly their role, we placed a thin (50 nm) AR coating (Si_3N_4) at the top of the cell. The AR coating was designed to work better around 500 nm wavelength where the sun maximum intensity is emitted. The first row in Table 3.1 shows a typical unit cell. It consists of an Ag back reflector, an amorphous silicon absorbing layer, a 10 nm thickness SiO_2 layer (used for surface passivation in the realistic cells) on top of silicon and an antireflection coating (Si_3N_4 of 50 nm thickness) at the top part of the structure.

Table 3.1| Simple solar cells with metal nanostructures of 2D periodicity.

Case 1	Case 2	Case 3

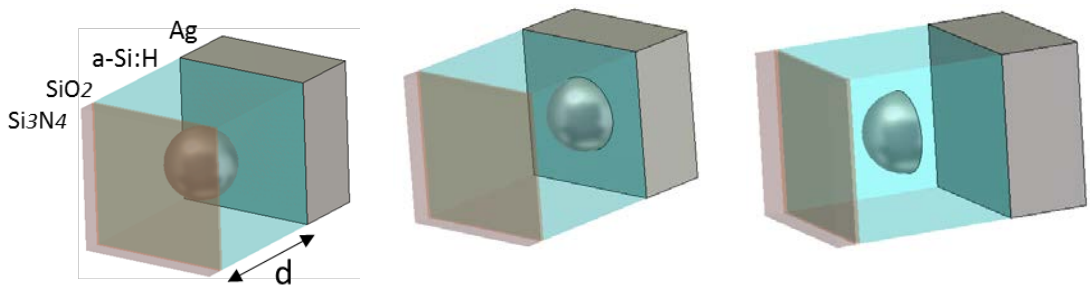

a) Nanostructure b) Radius c) Position d) Periodicity	J_{equiv} Enhancement factor over the reference structure	J_{equiv} (mA cm^{-2})	Ratio: J_{equiv} / J_{Yablo} %
Case 1: ***a) Spheres*:** ***b)*** 100 nm radius ***c)*** at d/2 ***d)*** 400 nm periodicity	1.72	17.4	77.2
Case 2: ***a) Hemispheres*:** ***b)*** 100 nm radius ***c)*** back reflector ***d)*** 400 nm periodicity	1.70	17.27	76.5
Case 3: ***a) Hemispheres*:** ***b)*** 100 nm radius ***c)*** at d/2 ***d)*** 400 nm periodicity	1.69	17.05	76.5

The equivalent photocurrent J_{equiv} *was calculated for the wavelength range between 300 and 1,100 nm. The* ***reference structure*** *consists of an Ag back reflector, a Si absorbing layer and a 10 nm* SiO_2 *surface passivation layer. The* J_{Yablo} *is the equivalent photocurrent for the absorption calculated by the theoretical limit.*

The absorption and photocurrent results in all other cases (cylindrical pillars, cubes) were inferior of those achieved with spheres and hemispheres, and the cubes gave the minimum absorption and photocurrent enhancement than all the nanostructures of different shape. The reason why spheres give better response when placed in the middle of the absorbing layer will be discussed after the Table 3.2.

Table 3.2| Simple solar cells with metal nanostructures of 1D periodicity for both polarizations, TE: (E//y) and TM: (H//y or E//x).

Hemi-Cylinders	Cylinders	Stripes
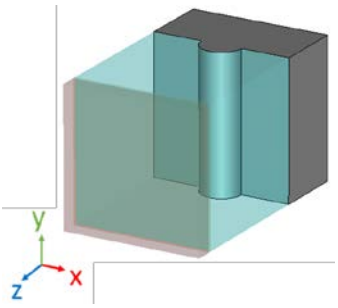	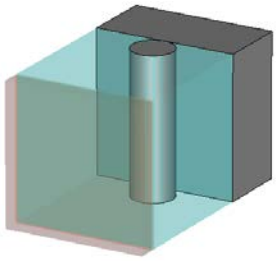	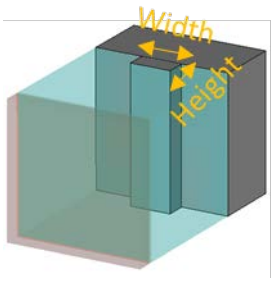

a) Nanostructure b) Dimensions c) Periodicity	J_{equiv} Enhancement factor over the reference	J_{equiv} (mA cm^{-2})	Ratio: J_{equiv} / J_{Yablo} %
a) ***Hemicylinders*:** ***b)*** 60 nm radius ***c)*** 400 nm periodicity	*Back reflector*: (TE) **1.71** (TM) **1.69** *Middle*: (TE) 1.68 (TM) 1.60	*Back reflector*: (TE) 17.23 (TM) 17.09 *Middle*: (TE) 17.04 (TM) 16.25	*Back reflector*: (TE) 76.30 (TM) 75.71 *Middle*: (TE) 75.52 (TM) 72.00
a) ***Cylinders*:** ***b)*** 60 nm radius ***c)*** 400 nm periodicity	*Back reflector*: (TE) **1.70** (TM) **1.68** *Middle*: (TE) 1.64 (TM) 1.64	*Back reflector*: (TE) 17.15 (TM) 17.03 *Middle*: (TE) 16.59 (TM) 16.60	*Back reflector*: (TE) 76.00 (TM) 75.47 *Middle*: (TE) 73.51 (TM) 73.60
a) ***Stripes*:** ***b)*** 120 nm width, 60 nm height ***c)*** 400 nm periodicity	*Back reflector*: (TE) **1.69** (TM) **1.59** *Middle*: (TE) 1.57 (TM) 1.51	*Back reflector*: (TE) 17.12 (TM) 16.10 *Middle*: (TE) 15.95 (TM) 15.33	*Back reflector*: (TE) 75.83 (TM) 71.30 *Middle*: (TE) 70.67 (TM) 67.92
a) ***Stripes*:** ***b)*** 120 nm width, 120 nm height ***c)*** 400 nm periodicity	*Back reflector*: (TE) **1.69** (TM) **1.62** *Middle*: (TE) 1.61 (TM) 1.53	*Back reflector*: (TE) 17.11 (TM) 16.40 *Middle*: (TE) 16.28 (TM) 15.50	*Back reflector*: (TE) 75.81 (TM) 72.60 *Middle*: (TE) 72.15 (TM) 68.7

The equivalent photocurrent J_{equiv} was calculated for the wavelength range between 300 and 1,100 nm. The ***reference structure*** *consists of an Ag back reflector, a Si absorbing layer and a 10 nm SiO_2 surface*

passivation layer. The J_{Yablo} *is the equivalent photocurrent for the absorption calculated by the theoretical limit.* ***Red*** *numbers show the best results for TE polarization for each structure, and the* ***green*** *numbers show the best results for TM polarization for each structure.*

From Table 3.2, it is clearly seen that for all the geometries the TE polarization (**E**//y) (red bold numbers) gave the best photocurrent enhancements. The reason is that the LSPRs are excited for TM polarization, mostly at the wavelengths where silicon does not absorb, so, the main effect is increased absorption from metal nanoparticles for these wavelengths that reduces the cell performance.

Moreover, spherical-like particles (cylinders and hemicylinders) always show better response than stripes (also different dimensions examined that we do not show here), both for TM and TE polarization and in every position inside the silicon layer.

Also, TE polarization for nanoparticles placed on the back reflector always show better response than TE and TM in every other position.

Interestingly, cylinders at the middle was the only case (for Si thickness: 400 nm) that TE absorption didn't exceed that for TM polarization. When the metal nanoparticles are placed at the middle of the absorbing layer they come closer to air and the effective refractive index of their environment lowers. As a result, their resonances shift to lower wavelengths where the silicon absorbs more.

Also, the hemicylinders at the back showed better TE response than cylinders at the back, but worse TM response when they were placed at the middle than cylinders at the middle.

In summary, at the middle of the solar cell, more symmetrical cylinder nanoparticles show better response than hemicylinders regarding the LSPR excitation. At the back reflector, hemicylinders show better TM and TE response than cylinders, resulting from the better coupling with the waveguide modes supported by the Si slab.

Therefore, we speculate that for 2D periodicity, the spheres at the middle gave the best results, since, 2D periodicity allows both for TE and TM polarization the excitation of LSPRs for normal incidence, and since the response of symmetrical nanoparticles at the middle is better when the LSPR is excited, spheres at the middle give the best results. In general though, the important finding of this work is that the photocurrents are always very close, indicating that the results are almost the same, no matter the shape of the nanoparticle.

The contour plot of the absorption enhancement as a function of period of the nanostructures which is shown in Fig. 3.2, strongly resembles the dispersion relation of the waveguide modes. The structure consists of an AR coating (with 50 nm thickness) on top, a SiO2 layer (with 10 nm thickness), and a silicon absorbing layer with 400 nm thickness on top of the Ag back reflector. Ag cylinders are periodically placed at the back reflector. The white lines show the orders of the propagating guided modes of the structure. The absorption enhancements are calculated by comparing with the reference structure which is the same with the previous structure but without the metallic nanoparticles and the AR coating. As one

can see, for TM polarization, the coupling is less strong in silicon [Fig. 3(c)], than for TE [Fig. 3(a)], because of the huge absorption inside the cylinders at the LSPRs [Fig. 3(d)], in agreement with the conclusions of Table 3.2. The period of 400 nm corresponds to the period with the maximum photocurrent that was found from the optimization.

Moreover, Fig. 3.3 shows the contributions of the AR coating and the periodic placed metallic nanoparticles to the absorption enhancements for different thicknesses of the absorbing layer. The reference structure, shown in the right inset of Fig. 3.3, consists of a 10 nm layer of SiO_2 (used for surface passivation in the realistic cells), an thin (50-400 nm) a-Si:H absorbing layer and a silver substrate which can work as an electrical back contact and reflector of incident light.

Each individual structure (AR only, nanoparticles only, AR and nanoparticles) was compared by integrating its absorption over the sun spectrum (AM 1.5G) and normalize it with the reference structure with the equivalent thickness. As one can see, the enhancements without the AR coating are very poor since the incident radiation is lost due to reflection, while the

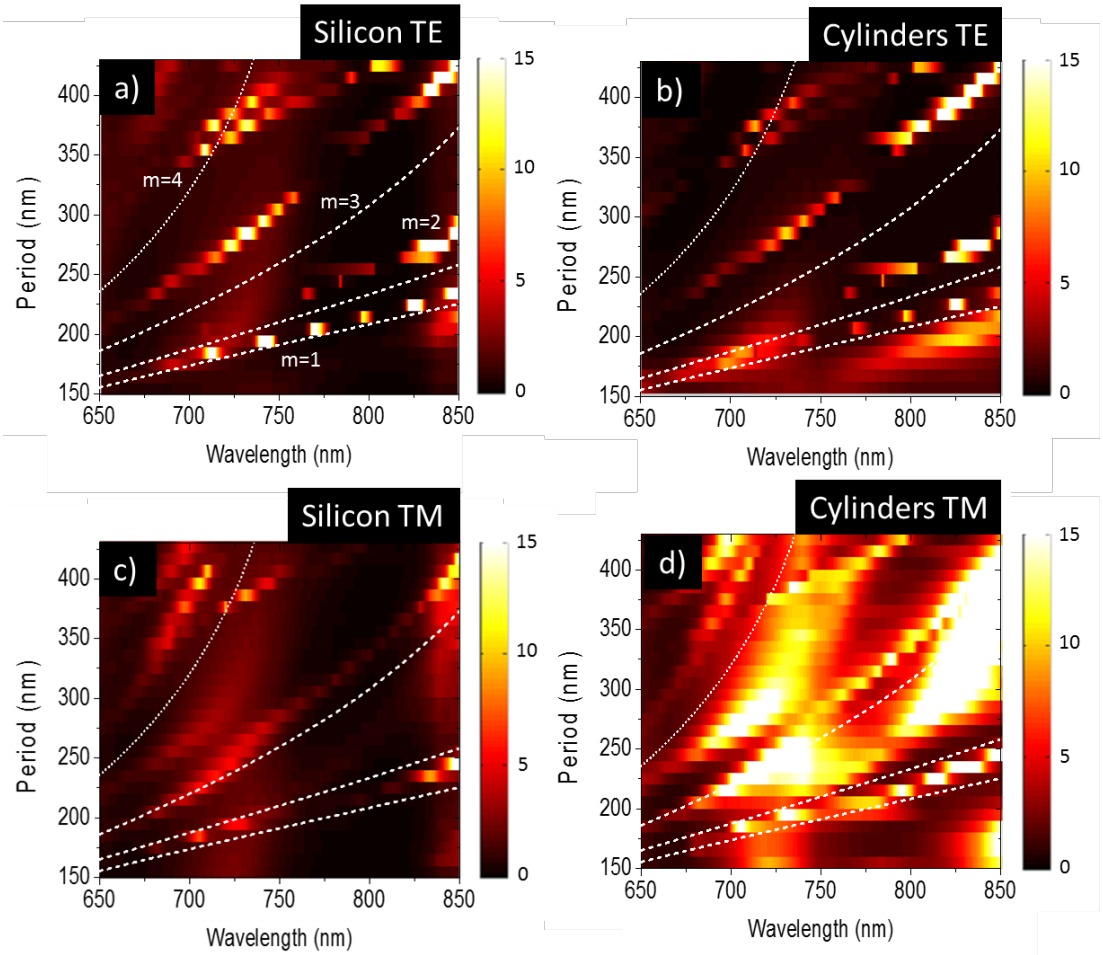

Fig. 3.2: *Contour plots showing the absorption enhancement (color bar) as a function of period and the wavelength. The structure consists of an AR coating (with 50 nm*

*thickness) on top, a SiO_2 layer (with 10 nm thickness), and a silicon absorbing layer with 400 nm thickness on top of an Ag back reflector. Ag cylinders are periodically (1D periodicity) placed at the back reflector. The absorption enhancements are calculated by comparing with the reference structure which is the same with the previous structure but without the metallic nanoparticles and the AR coating. The white lines show the orders of the propagating guided modes of the structure. (**a**) Absorption enhancement inside Si for TE polarization. (**b**) Absorption enhancement inside the Ag cylinders for TE polarization. (**c**) Absorption enhancement inside Si for TM polarization. (**c**) Absorption enhancement inside the Ag cylinders for TM polarization.*

combination of the metallic nanoparticles and the AR coating gives the best results. The current enhancements are shown for TE polarization (**E**//cylinders) which gave larger enhancements compared with TM, except for the case at which the absorbing layer had 50 nm thickness. For this case both the reduction of the radius of the optimized cylinder and the reduction of the thickness of the solar cell changed the environment for the metallic nanoparticles. As a result, the LSPRs blueshifted at the wavelengths where silicon absorbs and the current enhancement reached a value of almost 2.1 (top left black triangle in Fig. 3.3).

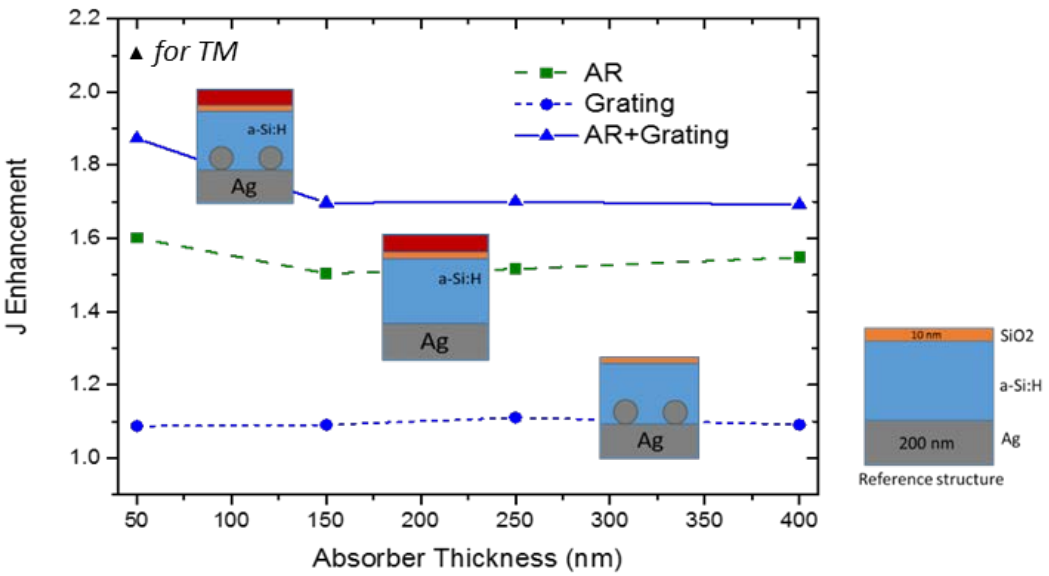

Fig. 3.3: *Photocurrent enhancement (compared to the reference structure) as a function of the absorber (Si) thickness for a system of silver cylinders (grating) on*

top of the back reflector, for a system without the cylinders but with antireflection (AR) coating and the system combining the cylinder and antireflection coating. E//cylinders. The picture demonstrates the role of a periodic grating of metal nanoparticles without and under the presence of an antireflection coating. One can see that the antireflection coating allows the maximum interaction of the incident radiation with the nanoparticles. Only for a Si thickness of 50 nm the TM polarization gave better results due to LSPRs, reaching a value of almost 2.1.

3.2.3 Exploiting Propagating Surface Plasmon Polaritons

3.2.3.1 Operational principles of SPPs

The second fundamental plasmonic excitation examined is SPPs which are propagating, non-radiative electromagnetic waves that are bound to the metallic-dielectric interface and are coupled to collective oscillations of the electrons in the metal [Fig 3.4(a)]. SPPs play a key role in many applications like solar cells, due to their relatively long propagation distance and strong confinement of the localized fields to the metal-dielectric interface. The absorption takes place at each material (either at the metal or the dielectric) according to their absorption coefficients.

It has been shown that periodically placed nanoparticles on top of the metallic surfaces, significantly scatter the incident energy and couple it to the SPP modes. More specifically, periodically nanostructured metallic surfaces serve as a diffraction grating and diffract light providing the excess momentum, k_{gx}, to compensate the wave-vector mismatch between incident wave-vector, k_{light}, and the surface plasmon polariton wave-vector, k_{spp}, as shown in Fig. 3.4(b).

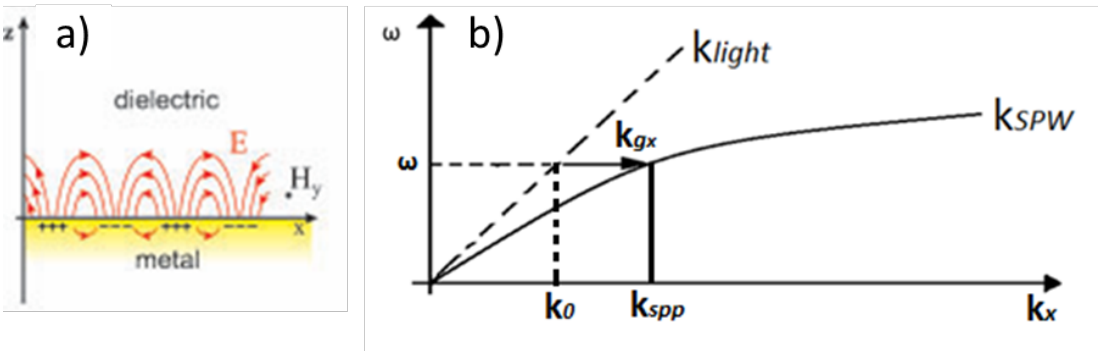

Fig. 3.4: ***(a)*** *Charge density oscillations at the metal/dielectric interface with the associated EM fields.* ***(b)*** *The dispersion relation of an SPP, illustrating the momentum mismatch between SPPs and photons that has to be overcome in order to excite them.*

The dispersion relation of the propagating SPPs at a metal-dielectric interface is given by the equation 3.1, where ε_m corresponds to the complex permittivity of the metal, ε_d is the complex permittivity of the infinite dielectric layer, k_{SPP} is the frequency dependent surface plasmon wave vector and k_0 is the free space wave-vector. The coupling mechanism is given by equation 3.2, where k_x is the in-plane component of light and m is an integer which corresponds to the diffracted order of the SPP. $k_{gx} = 2\pi L$ is defined as the grating wave number that shows the in-plane momentum given by the grating with period, L.

$$k_{SPP} = k_0 \sqrt{\frac{\varepsilon_m \cdot \varepsilon_d}{\varepsilon_m + \varepsilon_d}} \qquad (3.1)$$

$$k_{SPP} = k_x \pm m k_{g_x} \qquad (3.2)$$

Since the in-plane SPP possesses momentum higher than the momentum of the in-plane component of light, the SPP no longer matches the momentum of radiative light and it stays confined to the interface. However, the presence of the nanostructuring (nanoparticles) make SPP to undergo a scattering process, while it propagates along the in-plane interface, re-radiating it back into the direction of the zero reflected beam.

As a result, the shape and size of the metallic nanoparticles play an important role for both the excitation of the SPP mode as well as at the optical response of the system regarding the scattering procedure that channels energy back to the radiative zone.

The main problem though when exploiting the SPPs for a-Si:H based solar cells is the difficulty to control the wavelength of the SPP resonance and tune it at the wavelengths that matter regarding absorption enhancements. The reason is that the material that is used in this work is a dispersive material and therefore equation 3.1 changes for every wavelength. In addition, the refractive index of a-Si:H was always large and the excitation of the SPP occured always at higher wavelengths where silicon does not absorb and as a result no substantial enhancements were observed.

However, studies[38] have shown that SPPs can provide substantial absorption enhancements to polymer, perovskite etc. based solar cells which have lower refractive index than silicon and also absorb more efficiently at the SPP resonance. In the following subsection we provide the operational principles both theoritically and experimentally (Dr. G. Kenanakis).

3.2.3.2 Results exploiting SPPs

The typical structure that was studied is shown in the inset of Fig. 3.5, consisting of a metallic thin film (Ag) with a periodic grating of Ag stripes on top. One can see the geometrical features of the structure in the caption of Fig. 3.5. The theoretical study (simulations) of our the structure was performed using the Frequency Domain Solver of the JCM suite software, while Ag is the active metal with a complex permittivity which is described by the lossy Drude model with ω_p=13.20·10^{15} and γ=43.33·10^{13}.

The experimental EM characterization of the structure (Dr. G. Kenanakis) was performed in the frequency regime 400-900 nm through transmission and reflection measurements, using a Bruker Vertex 70v Fourier-transform infrared spectrometer (with a collimated beam) and two fused silica ultra-broadband linear wire grid polarizers.

Fig. 3.5 shows for normal incidence and TM polarization (electric field normal to the stripes), the first order diffraction excitation process of the SPP which is manifested as a reflectivity minimum (and thus an absorption peak) in the zero order reflection from the structure of Fig. 3.5. For a binary silver grating in air with dimensions that slightly perturb [blue line in Fig. 3.5(a)] the planar dispersion relation (equation 3.1) of the propagating mode at the metal-dielectric interface, the wavelength of the plasmon resonance is found to be at 429 nm, i.e., very close to the expected one at 424nm calculated from equation 3.1. It is clearly seen that by further manipulation of the geometric parameters of the structure, one can tune both the width and the height of the absorption resonance peak.

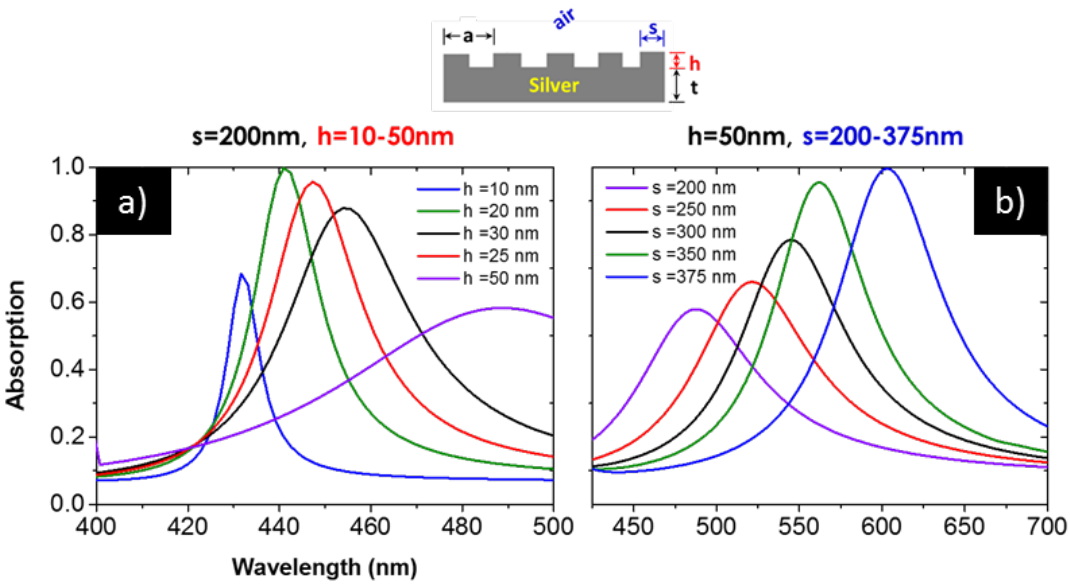

Fig. 3.5: *Absorption spectra for normal incidence and TM polarization (electric field normal to the stripes), of the structure under investigation, for a given width of the grating component (s=200 nm) and several values of height, h (**a**), and for a given height of the grating component (h=50 nm) and several values of width, w (**b**). In the*

inset of Fig. 1, one can see the proposed structure which consists of a silver thin film with a thickness t of 200 nm, and a periodic silver grating with the geometry mentioned above. In all cases the unit cell, a, of the structures is 400 nm.

Fig. 3.6 illustrates [for the absorption peaks shown in Fig. 3.5(a)] the accossiated (numerically simulated) band gaps (magnitude of the bandgaps) and the shifts of the plasmon resonance wavelength (position of the band edges), as we increase the geometry parameters and the dispersion relation is further perturbed[39,40,41]. The bandgap opens when counter propagating SPPs at the metal-dielectic interface, that were efficiently Bragg scattered by the Ag stripes (nanostructure on top of metal), meet with each other. Two SPP standing waves are formed associated with different energies (because they stand at different geometrical positions), and between these energies the SPP propagation is forbidden due to destructive interference.

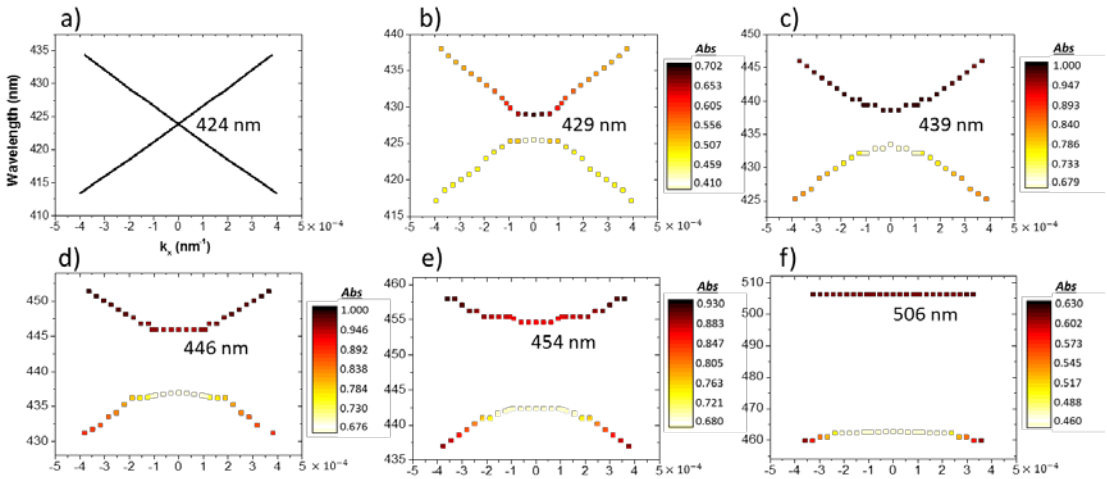

Fig. 3.6: ***(a)*** *Planar case, i.e. Ag film without stripes. [(**b**)-(**f**)] Magnitude and position of the bandgaps as we change the height (h) from 10nm to 50nm, of the stripes for the structure shown in Fig. 3.5 (with a=400nm, s=200nm), and the resulting coupling of light to the band edges as shown in the absorption plot to the right of each graph. The y axis shows the wavelength and the x axis shows the parallel component of the incident wave vector.*

For the binary grating examined here, one can see in Fig 3.6[(b)-(f)] only one branch which corresponds to a single absorption peak [see in Fig.3.5(a)], because, incident light couples[42] only with the low energy SPP standing wave, whose associated field distribution is shown in Fig. 3.7.

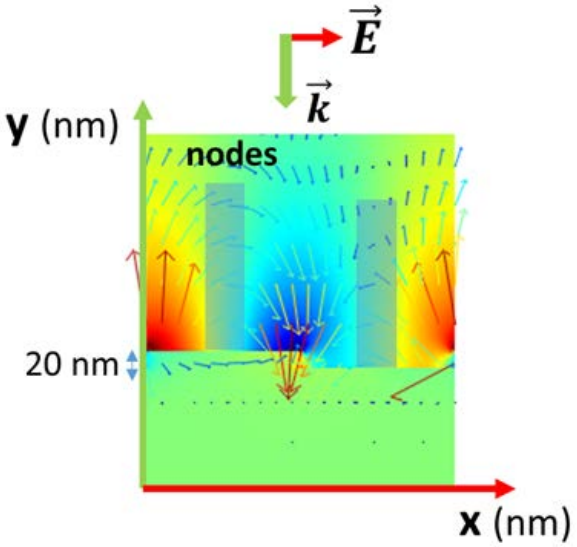

Fig. 3.7: *Electric field (y-component) at 439nm showing the coupled standing wave SPP with the incident light for the binary grating with a=400nm, s=200nm, h=20nm (see Fig. 3.5) i.e., the case of Fig. 3.6(c).*

Furthermore, as shown in Fig. 3.5(a), the absorption initially increases with increasing the height, *h*, of the Ag stripes, until a critical point. At this point, the radiation reflected directly from the surface (the zeroth diffracted order) and the radiation out-coupled (scattered back to the radiation zone) from the SPP are equal and exactly out of phase leading to zero reflection and maximum absorption. After the critical coupling, the two components again do not sum to zero increasing the reflection at the cost of the absorption. The width of the absorption resonance also increases with *h* due to the total damping of the oscillator.

By changing then the width, *s*, of the stripe [Fig. 3.5(b)] the strength of the absorption resonance starts to increase again, while the width of the resonance slightly decreases. The behavior of the plasmon resonance peak is determined by the presence and the size of the Fourier harmonics of the Fourier transformation equation 3.3 of the binary grating:

$$f(x) = \frac{4}{\pi} \cdot \left(A \cdot sin\left(1 \cdot k_{gx} \cdot x\right) + \frac{A}{3} \cdot sin\left(3 \cdot k_{gx} \cdot x\right) + \frac{A}{5} \cdot sin\left(5 \cdot k_{gx} \cdot x\right) + ..\right) \quad (3.3)$$

where *A* is the Fourier coefficient [for a pure sinusoidal grating (i.e. one Fourier harmonic) *A* would be its amplitude, which is related to the scattering efficiency of the grating], and $k_{gx}=2\pi/L$ is defined as the grating wave number that shows the in-plane momentum given by a grating with period, *L*.

Since we have only two degrees of freedom (the width and the height of the stripe) for a binary grating of a given periodicity, when we change the width or the height of the stripe, the Fourier coefficients change accordingly, affecting the plasmon resonance absorption peak. In general, the contributions of each Fourier harmonic (*A*, *A/3*, *A/5*, ...) play a role regarding SPP excitation, zero order reflection, re-radiation of the SPPs, band gap formation etc.

Finally, in Fig. 3.8, we present both the theoretical and the experimental spectra regarding the silver grating of 50 nm height, 350 nm width and a period of 400 nm. As one can see, both theory and experiment demonstrate a perfect absorption peak located at 603 nm.

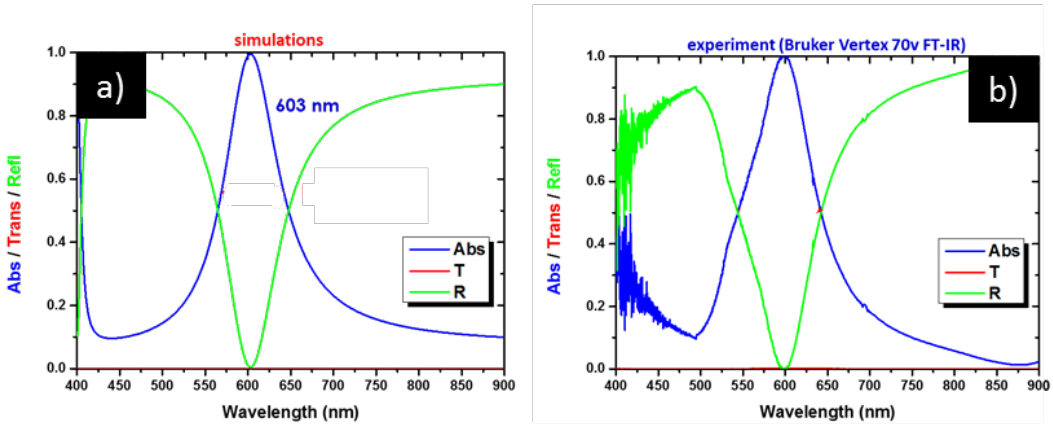

Fig. 3.8: *Theoretical (**a**) and experimental (**b**) reflection (green), transmission (red), and absorption (blue) spectra for the grating presented in the top inset of Fig. 3.5, the case of Fig. 3.5(b) blue line.*

However, as we discussed in subsection *3.2.2.1*, noteworthy absorption enhancements regarding SPPs for a-Si:H based solar cells (a-Si:H instead of air on top of the Ag grating) could not be achieved due to the manifestation of the SPP phenomenon only to higher wavelengths where silicon does not absorb.

3.3 Conclusions

In summary, we have shown that the enhanced absorption in a-Si:H solar cells with embedded periodic systems of metalic nanoparticles is mostly because of the waveguide modes that are excited by the periodicity of the metallic nanoparticles, while for both types of coupling of the incident radiation with those guided modes, i.e. coupling due to the scattering of the diffraction grating created by the nanoparticles or due to the LSPRs of isolated nanoparticles, spherical nanoparticles showed the best response among all the nanoparticle shapes studied.

For nanoparticles of 1D periodicity, the results concerning absorption enhancement and photocurrent achieved were always better (both for TE and TM polarization) for spherical and hemispherical nanoparticles on top of the back reflector, while better response for TM polarization was shown for symmetrical spherical nanoparticles (cylinders) at the middle of the absorbing layer than hemisymmetrical like hemispheres or hemicylinders.

For nanoparticles of 2D periodicity, the photocurrent enhancements were the maximum for spherical nanoparticles at the middle of the solar cell, and for hemispheres at the back reflector.

Finally, SPP modes of the metal-dielectric interface of the solar cell could not provide noteworthy absorption enhancements for a-Si:H based cells, but we showed their potential for solar cells with different absorbing layers like polymers, perovskites etc.

4 Dielectric nanostructures on top of the absorbing layer

4.1 Introduction

As it was discussed in Chapter 3, reflection that occurs at an air–silicon interface plays an important role for enhancing the performance of solar cells. Therefore, the development of antireflection schemes, which aim to cancel such reflection, is important. For example, in conventional thick crystalline silicon solar cells, micron-sized pyramidal surface texturing is used[43]. The angular randomization of the scattered light at the surface can increase light absorption up to a factor[44] of $4n^2$ due to multiple light scattering, and subsequently provides a reduction in reflection. However, in thin film solar cells, micron-sized texturing is not possible. In this work, we attempted to eliminate reflection with subwavelength silicon nanostructures on top of the cells. Such nanostructures possess Mie resonances with associated big scattering and absorption cross-sections.

It has been demonstrated[45] that periodic arrays of resonant, subwavelength, high index dielectric objects placed at an air–material interface can significantly reduce reflection. This is attributted to many reasons like, the gradual change of the refractive index from air to silicon[46], multiple light scattering[47] where the nanostructure arrays enhance the scattering path length, or coupling of Mie resonances with the substrate, since, high index nanostructures feature a similar scattering albedo as metallic nanostructures without the parasitic optical losses.

Here, we investigate a-Si:H nanostructures on top of thin a-Si:H absorbing layers and we demonstrate that the absorption and scattering resonaces of the nanostructures can effectivelly couple with the silicon substrate providing broadband absorption enhancements, reaching the theoritical limit.

4.2 Results and discussion

Nanostructures can be made in a variety of shapes and sizes which can significantly influence optical properties of the solar cell. In this work the optical properties of nanocone, nanocylinder, nanocube and nanodisk arrays on top of thin Si layers were examined. Some examples of the unit cells are shown in Fig. 4.1, along with the parameters that define these structures. BD is the base diameter that touches the Si substrate for nanoparticles like cones, D is the diameter for cylinders and P is the period of the arrays.

By simulating the absorption, reflection, transmission spectra and the electric field distributions of the silicon nanostructures on Si, we show the strong influence of the Mie resonances on high absorption over a wide spectrum.

Examples of the nanoparticle operation is shown in Fig. 4.1(b) which shows the electric field at the second resonance of the nanoparticle geometry for a silicon sphere in air and for different geometries of silicon nanoparticles on top of the silicon substrate. As a result, when at resonance, this type of structures exhibit both the forward preferential scattering, that we

have met also for silver nanoparticles on top of the absorbing layer, and the substrate-Mie-coupling due to the introduction of leaky channels into the substrate for the light that is resonantly confined in the particle. By changing the diameter and size of the nanoparticle, the Mie resonances can be tuned and have the desired optical effect.

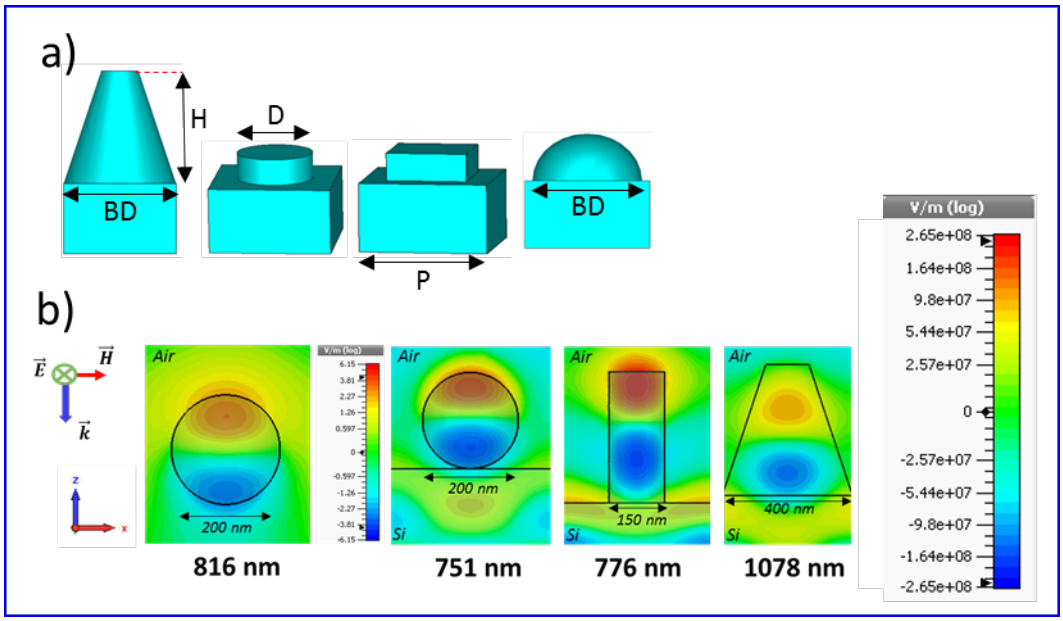

Fig. 4.1: *(**a**) Typical structures with antireflection properties that consist of subwavelength silicon nanoparticles (cones, nanocylinders, parallelograms, nanodisks) on top of the absorbing layer. (**b**) Nano-cavity resonance for a silicon sphere in air and different geometries of silicon nanoparticles (in arrays) on top of the silicon substrate. The y-component of the electric field is shown.*

In order to investigate this coupling further, in Fig. 4.2(a) we show the reflection spectrum for arrays of nanocylinders with P=400nm, H=350nm, an absorbing layer with 250 nm thickness (without a back reflector, the structure is in air), and different nanoparticle diameters (150, 250 and 300 nm), for normal incidence. The reflection from a bare silicon (black line) slab with equivalent thickness is also shown for comparison.

It is clearly seen that the reflection is significantly reduced due to the dielectric nanoparticles. The reason for that is the Mie resonances of the nanoparticles. The deeps in reflectivity at wavelengths 420, 510 and 554 nm as we increase the diameter is the characteristic behavior of the resonances that redshift with increasing the particle size. The strong coupling of light with the modes of the Si substrate when on resonance is explained by the strong forward scattering of light into the Si substrate from the Mie resonant nanoparticles, due to the high optical mode density of the high index silicon substrate.

The phenomenon at which the wavelength of resonance changes with the diameter can be greatly exploited in the case of conical shapoe, where Mie resonances could be excited for a broad range of wavelengths, since, always they could find an effective diameter. As a result,

in Fig. 4.2(b) we can see the enhanced antireflection properties of an optimized cone (blue line), (P=400nm, BD=400nm, top diameter=BD/6, H=400nm) compared to an optimized cylinder (black line), (P=400nm, D=250nm, H=100nm).

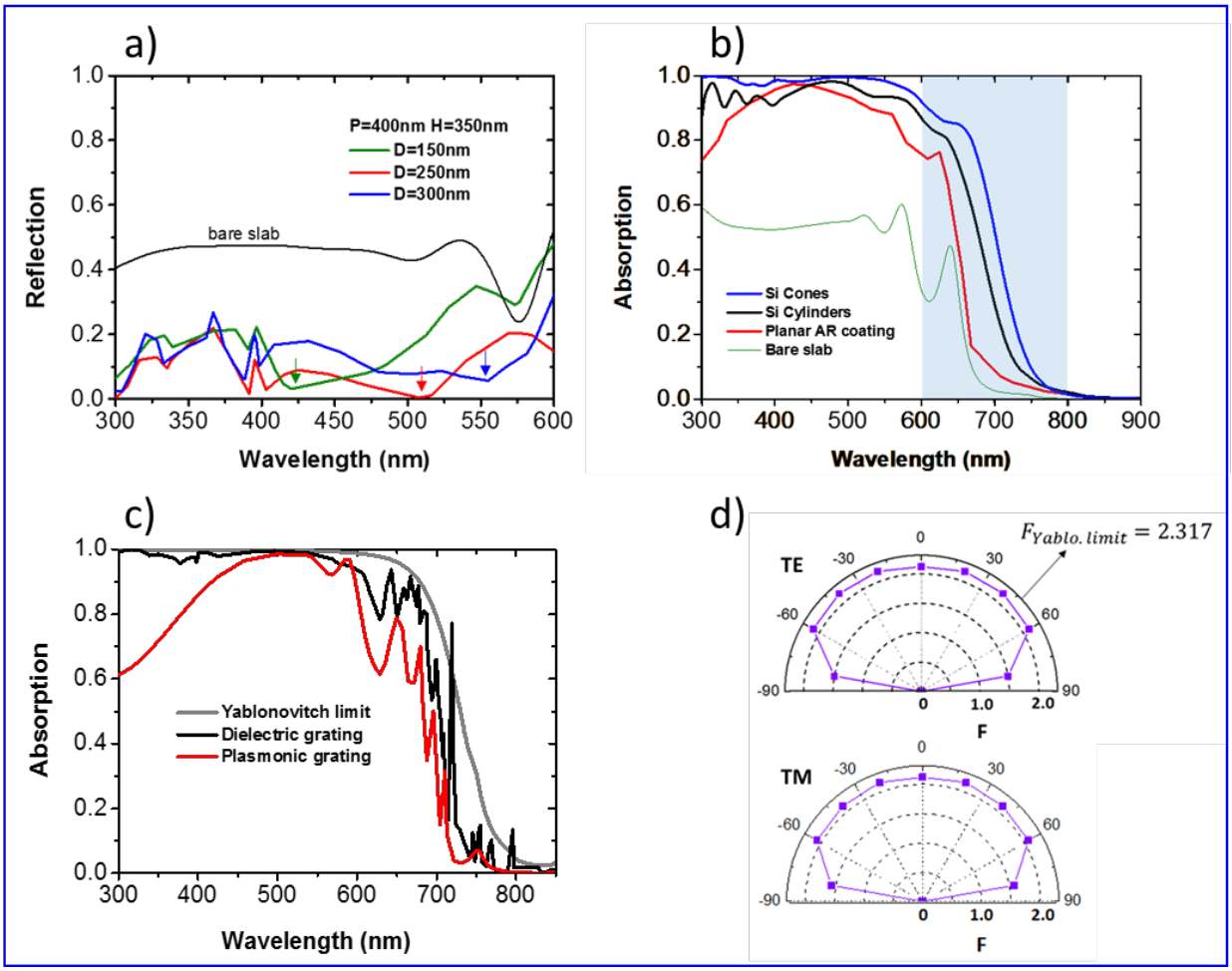

Fig. 4.2: *(**a**) Reflection spectrum (normal incidence) for structures with Si nanocylinders on top [geometry shown in Fig. 4.1(a), second case], of different diameters and fixed P=400nm and H=350nm. The arrows show the reflection deeps that correspond to the redshift of the Mie resonances as the diameter of the nanoparticle is increased. (**b**) Absorption in silicon for: i) Cut-Cones (blue line) [geometry shown in Fig. 4.1(a), first case], with BD=400nm, top diameter=BD/6, H=400nm. ii) Nanocylinders (black line) [geometry shown in Fig. 4.1(a), second case], with D=250nm, H=100nm. iii) Planar AR coating (Si_3N_4), and a bare slab for comparison. (**c**) Absorption spectrum comparison between the cut-cones of case (b) and the plasmonic based solar cell with arrays of Ag spheres inside the absorbing layer, and an AR coating on top, examined in Chapter 3 in subsection 3.2.1.2. (**d**) Angular dependence of the integrated absorption enhancement factor, F, (compared with a bare silicon slab with the same equivalent thickness). F equals to 2.12 for up to 60° angle of incidence, compared with*

$F_{Yablo.Limit}$ *which equals with 2.317.*

It is noted that both structures are on top of a thin absorbing layer with 250 nm thickness, wihout the Ag back reflector (in air), and they give almost the same results with the cases when the back reflector is placed, indicating that the light is well-trapped due to total internal reflection.

Moreover, in Fig. 4.2(c) one can see the enhanced absorption compared with a planar AR coating (Si_3N_4) which has less broad, wavelength-dependent antireflection properties. Additionally, such structures with arrays of silicon nanocylinders and nanocones provide enhanced light-trapping at the wavelengths were silicon absorbs poorly (600-800nm) compared with the planar antireflection coating, and their effectiveness at these wavelengths overcomes also plasmonic gratings that are placed inside the absorbing layer as shown in Fig. 4.2(c) where the theoretical Yablonovitch limit is also shown (gray line), calculated assuming perfect antireflection and perfect light trapping, for a slab with the equivalent thickness of the structure with the cones and the plasmonic structure. Fig. 4.2(d) shows that the Yablonovitch limit, for this kind of structures, can be reached, since for angles of incidence up to 60 degrees, absorption almost reaches the theoritical limit.

The curves in Fig. 4.2(b) are averaged (Adjacent-Averaging in Origin, weighted average on, 72 points of Window) in order to make the comparison easier; the dense peaks shown in Fig. 4.2[(a)-(b)] for wavelengths of 400nm and lower are attributed to the periodicity of the nanoparticles.

To illustrate the antireflection properties of the structures studied and to compare them, we show in Fig. 4.3 how the tendency for enhanced antireflection is dictated by the geometry of the silicon nanoparticles. The black numbers at each graph correspond to the integrated absorption for wavelengths 400-1100nm and the dark red percentages show the fraction of light absorbed (%) versus the theoretical limit calculated for silicon slabs with the equivalent thickness to that of the geometry at each case.

As one can see, the requirements for enhanced antireflection properties are big enough nanostructures (larger sizes than 100 nm) that can exhibit Mie resonances also at higher wavelengths (higher than 600 nm), so, a big fill factor is needed without approaching though the last cases where the structure is close to that of a planar surface. Moreover, the height itself plays a role in coupling with the substrate. Big heights are more decoupled from the substrate, so, they exhibit less broad Mie resonances (less leaky channels of the resonance to the substrate).

All essential requirements for antireflection, both big filling factors and diameter variation, are fulfilled by conical shaped nanoparticles, and consequently they provide the best results.

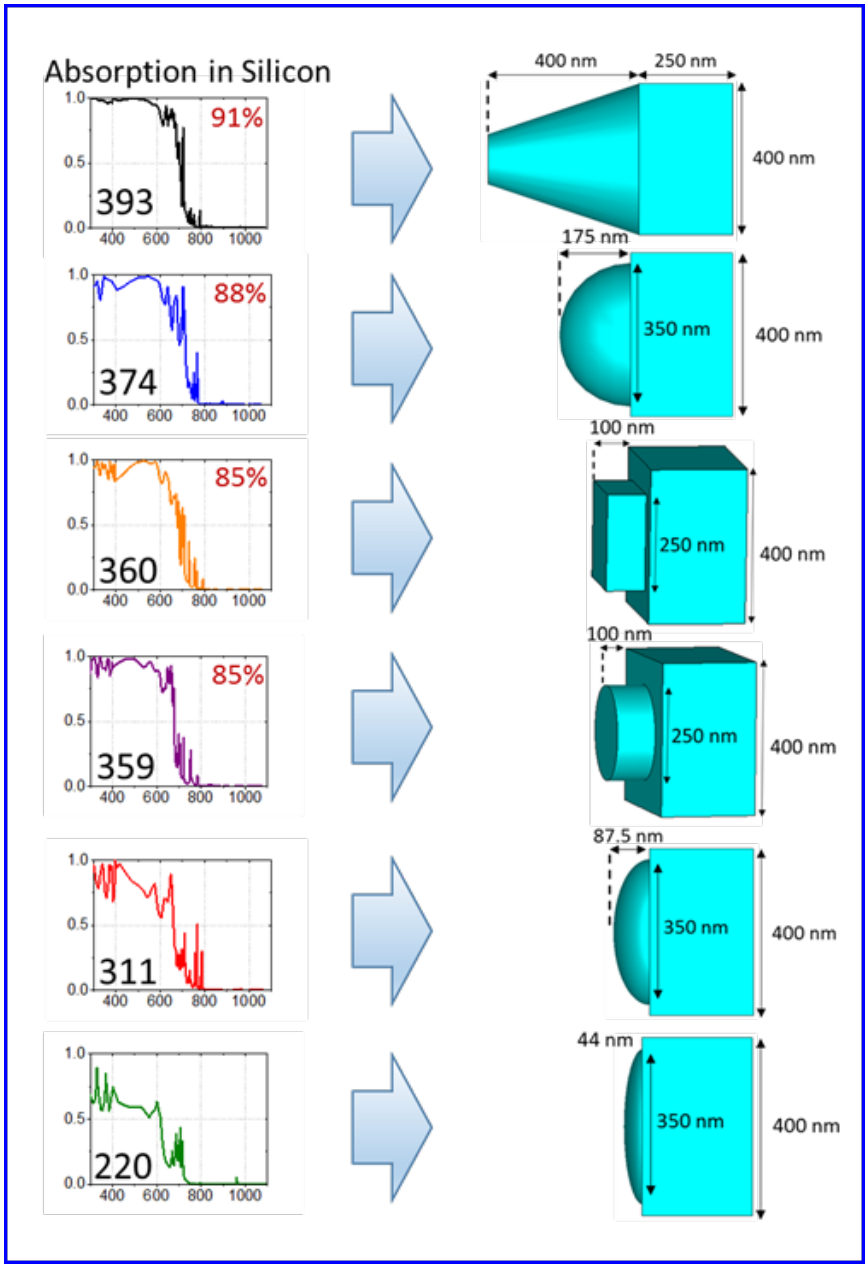

Fig. 4.3: *Absorption inside silicon for each geometry shown in the right column. The black numbers inside each graph show the integrated absorption, for wavelengths from 300 to 1100nm. The dark red percentages show the fraction of light absorbed (%) versus the theoretical limit, calculated for silicon slabs with the equivalent thickness to that of the geometry at each case.*

Another important parameter for designing solar cells and targeting to enhance absorption with this kind of nanostructures, is the position inside the solar cell, at which the absorption takes place. In Fig. 4.4 red lines correspond to the absorption inside the silicon nanoparticles and green lines to the absorption inside the silicon substrate. As the size of the nanoparticle increases, also the absorption in it increases too for lower wavelengths. Since, the absorption inside a-Si:H is very high for lower wavelengths, if the reflection is suppressed, the light can

easily be absorbed by the nanostructure. For larger nanoparticles, light travels larger distances inside the nanoparticle and is absorbed more efficiently according to the absorption coefficient of Si which is very high for lower wavelengths. Whereas, at higher wavelengths where silicon absorbs poorly, the substrate plays an important role, due to the need for light to be trapped at the waveguide modes.

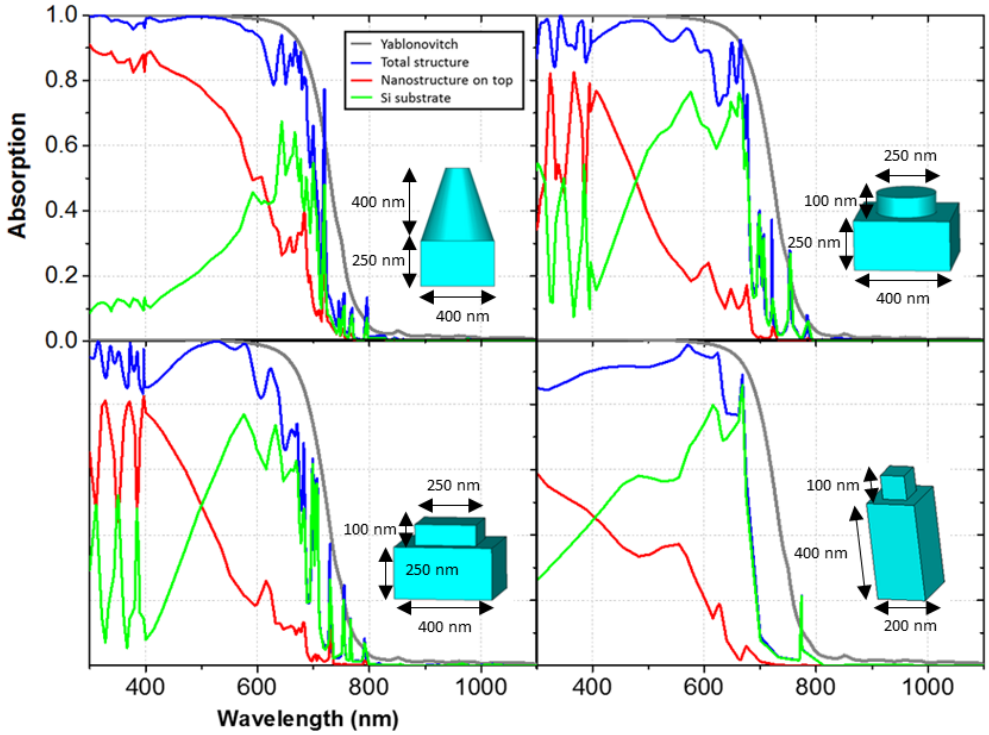

Fig. 4.4: *Shape effect of the silicon nanostructures on solar cell top. Such nanostructures can act as antireflection coatings increasing the solar radiation captured by the cell and thus its absorption. Among the different-shape particles that were examined the highest absorption was achieved for conical-shape nanostructures. The curves in the figure show the maximum absorption dictated by ray optics, known as Yablonovitch limit (gray lines), the total absorption in silicon (blue lines), while the red and green lines separate the Si absorption to that of the nanostructure (red lines) and the "substrate" (green lines).*

4.3 Conclusions

In summary, arrays of silicon nanostructures with various shapes and sizes placed on top of thin film silicon solar cells were investigated by simulations, and the best conditions as to achieve high solar cell absorption regarding their shape and size were shown. These subwavelength resonant Mie scatterers on top of the silicon thin film absorbing layers cause the reflection of light almost to vanish, providing broadband absorption enhancements. Both

the electric field distributions and the scattering cross sections associated with the Mie resonances of the nanostructures caused the coupling of the Mie resonance modes with the silicon substrate and the subsequent strong trapping of light at the waveguide modes of the Si substrate at the higher wavelengths (i.e. $\lambda > 600$ nm) where silicon absorbs poorly. Since, the Mie resonant wavelengths can be tuned by changing the diameters of the nanoparticles, and since nanocone structures provide a variable structure diameter, nanocones were proven the best structures (among the ones studied) for achieving large and broadband absorption.

Bibliography

[1] Williams, Richard. "Becquerel photovoltaic effect in binary compounds." The journal of Chemical physics 32.5 (1960): 1505-1514.
[2] Atwater, Harry A., and Albert Polman. "Plasmonics for improved photovoltaic devices." Nature materials 9.3 (2010): 205-213.
[3] Yablonovitch, Eli. "Statistical ray optics." JOSA 72.7 (1982): 899-907.
[4] Joulain, Karl, et al. "Definition and measurement of the local density of electromagnetic states close to an interface." Physical Review B 68.24 (2003): 245405.
[5] Sheng, Ping, A. N. Bloch, and R. S. Stepleman. "Wavelength-selective absorption enhancement in thin-film solar cells." Applied Physics Letters 43.6 (1983): 579-581.
[6] Gee, Jamek M. "Optically enhanced absorption in thin silicon layers using photonic crystals." Photovoltaic Specialists Conference, 2002. Conference Record of the Twenty-Ninth IEEE. IEEE, 2002.
[7] Schiff, Eric A. "Thermodynamic limit to photonic-plasmonic light-trapping in thin films on metals." Journal of Applied Physics 110.10 (2011): 104501.
[8] Callahan, Dennis M., Jeremy N. Munday, and Harry A. Atwater. "Solar cell light trapping beyond the ray optic limit." Nano letters 12.1 (2012): 214-218.
[9] Yu, Zongfu, Aaswath Raman, and Shanhui Fan. "Fundamental limit of nanophotonic light trapping in solar cells." Proceedings of the National Academy of Sciences 107.41 (2010): 17491-17496.
[10] Kelly, K. Lance, et al. "The optical properties of metal nanoparticles: the influence of size, shape, and dielectric environment." The Journal of Physical Chemistry B 107.3 (2003): 668-677.
[11] Barnes, William L., Alain Dereux, and Thomas W. Ebbesen. "Surface plasmon subwavelength optics." Nature 424.6950 (2003): 824-830.
[12] JCM Suite, http://www.jcmwave.com/
[13] CST Microwave Studio, http://www.cst.com.
[14] Francisco Javier Sayas. “A gentle introduction to the Finite Element Method.” (2008)
[15] Hoffmann, Johannes, et al. "Comparison of electromagnetic field solvers for the 3D analysis of plasmonic nanoantennas." SPIE Europe Optical Metrology. International Society for Optics and Photonics, 2009.
[16] Kelly, K. Lance, et al. "The optical properties of metal nanoparticles: the influence of size, shape, and dielectric environment." The Journal of Physical Chemistry B 107.3 (2003): 668-677.
[17] Bohren, Craig F., and Donald R. Huffman. Absorption and scattering of light by small particles. John Wiley & Sons, 2008.
[18] Young, Andrew T. "Rayleigh scattering." Applied Optics 20.4 (1981): 533-535.
[19] Wang, Ken Xingze, et al. "Absorption enhancement in ultrathin crystalline silicon solar cells with antireflection and light-trapping nanocone gratings." Nano letters 12.3 (2012): 1616-1619.
[20] Yablonovitch, Eli. "Statistical ray optics." JOSA 72.7 (1982): 899-907.
[21] Yablonovitch, Eli, and George D. Cody. "Intensity enhancement in textured optical sheets for solar cells." Electron Devices, IEEE Transactions on 29.2 (1982): 300-305.
[22] Green, Martin A. "Lambertian light trapping in textured solar cells and light-emitting diodes: analytical solutions." Progress in Photovoltaics: Research and Applications 10.4 (2002): 235-241.
[23] Schropp, R. E. I., and M. Zeman. "Amorphous ans microcrystalline silicon solar cells: modeling, materials and device technology (electronic Materials: Sciences & Technology)." (1998).
[24] Yang, Jeffrey C. "Advances in amorphous silicon alloy technology—the achievement of high-efficiency multijunction solar cells and modules." Progress in Photovoltaics: Research and Applications 6.3 (1998): 181-186.
[25] Soller, Brian J., Howard R. Stuart, and Dennis G. Hall. "Energy transfer at optical frequencies to silicon-on-insulator structures." Optics letters 26.18 (2001): 1421-1423.
[26] Dr. Matthias Zilk Jena
[27] Palik data silver, http://refractiveindex.info/
[28] Krenn, J. R., et al. "Squeezing the optical near-field zone by plasmon coupling of metallic nanoparticles." Physical Review Letters 82.12 (1999): 2590.
[29] Kottmann, Jörg P., and Olivier JF Martin. "Retardation-induced plasmon resonances in coupled nanoparticles." Optics Letters 26.14 (2001): 1096-1098.

[30] Hägglund, Carl, et al. "Electromagnetic coupling of light into a silicon solar cell by nanodisk plasmons." Applied Physics Letters 92.5 (2008): 053110.
[31] Spinelli, P., et al. "Controlling Fano lineshapes in plasmon-mediated light coupling into a substrate." Optics express 19.103 (2011): A303-A311.
[32] Luk'yanchuk, B. S., et al. "Extraordinary scattering diagram for nanoparticles near plasmon resonance frequencies." Applied Physics A 89.2 (2007): 259-264.
[33] Lim, S. H., et al. "Photocurrent spectroscopy of optical absorption enhancement in silicon photodiodes via scattering from surface plasmon polaritons in gold nanoparticles." Journal of Applied Physics 101.10 (2007): 104309.
[34] William L. Barnes, Alain Dereux & Thomas W. Ebbesen, Surface plasmon subwavelength optics, University of Exeter, EX4 4QL, UK, Nature Publishing Group, 2003.
[35] Jung Hyeun Kim, Sheryl H. Ehrman, George W. Mulholland and Thomas A. Germer, "Polarized light scattering by dielectric and metallic spheres on silicon wafers", Published in Applied Optics 41(25), 5405-5412 (2002)
[36] Sheng P, Bloch AN, Stepleman RS (1983) Wavelength-selective absorption enhancement in thin-film solar cells. Appl Phys Lett 43:579–581.
[37] Jeremy N. Munday, Harry A. Atwater, "Large Integrated Absorption Enhancement in Plasmonic Solar Cell by Combining Metallic Gratings and Antireflection Coatings", Nano Lett., American Chemical Society, 2011
[38] Yang Yang, Gang Li , "Progress in High-Efficient Solution Process Organic Photovoltaic Devices: Fundamentals, Materials, Devices and Fabrication", Topics in Applied Physics 130, Springer-Verlag Berlin Heidelberg, 2015
[39] R.C. McPhedran, M.D. Waterworth, Properties of diffraction grating anomalies. Opt. Acta 20, 533–547 (1973)
[40] H. Raether, in Surface Plasmons on Smooth and Rough Surfaces and on Gratings. Springer Tracts in Modern Physics, vol. 111 (Springer, New York, 1988)
[41] I. Pockrand, H. Raether, Surface plasma-oscillations in silver films with wavy surface profiles—quantitative experimental study. Opt. Commun. 18, 395–399 (1976)
[42] Barnes, W. L., et al. "Physical origin of photonic energy gaps in the propagation of surface plasmons on gratings." Physical Review B 54.9 (1996): 6227.
[43] Han, Yangang, et al. "Formation of various pyramidal structures on monocrystalline silicon surface and their influence on the solar cells." Journal of Nanomaterials 2013 (2013): 7.
[44] Wang, Ken Xingze, et al. "Absorption enhancement in ultrathin crystalline silicon solar cells with antireflection and light-trapping nanocone gratings." Nano letters 12.3 (2012): 1616-1619.
[45] Evlyukhin, A. B., Reinhardt, C. & Chichkov, B. N. Multipole light scattering by nonspherical nanoparticles in the discrete dipole approximation. Phys. Rev. B 84, 235429 (2011).
[46] Zhu, J. et al. Optical absorption enhancement in amorphous silicon nanowire and nanocone arrays. Nano Lett. 9, 279–282 (2008).
[47] Muskens, O. L., Rivas, J. G., Algra, R. E., Bakkers, E. P. & Lagendijk, A. Design of light scattering in nanowire materials for photovoltaic applications. Nano Lett. 8, 2638–2642 (2008).